ASA, CSSA, and SSSA Virtual Issue Call for Papers:

Advancing Resilient Agricultural Systems: Adapting to and Mitigating Climate Change

Content will focus on resilience to climate change in agricultural systems, exploring the latest research investigating strategies to adapt to and mitigate climate change. Innovation and imagination backed by good science, as well as diverse voices and perspectives are encouraged. Where are we now and how can we address those challenges? Abstracts must reflect original research, reviews and analyses, datasets, or issues and perspectives related to objectives in the topics below. Authors are expected to review papers in their subject area that are submitted to this virtual issue.

Topic Areas

- Emissions and Sequestration
  - » Strategies for reducing greenhouse gas emissions, sequestering carbon
- Water Management
  - » Evaporation, transpiration, and surface energy balance
- Cropping Systems Modeling
  - » Prediction of climate change impacts
  - » Physiological changes
- Soil Sustainability
  - » Threats to soil sustainability (salinization, contamination, degradation, etc.)
  - » Strategies for preventing erosion
- Strategies for Water and Nutrient Management
  - » Improved cropping systems
- Plant and Animal Stress
  - » Protecting germplasm and crop wild relatives
  - » Breeding for climate adaptations
  - » Increasing resilience
- Waste Management
  - » Reducing or repurposing waste
- Other
  - » Agroforestry
  - » Perennial crops
  - » Specialty crops
  - » Wetlands and forest soils

Climate Change Virtual Issue

Submit Now!

Deadlines

Abstract/Proposal Deadline: Ongoing
Submission deadline: 31 Dec. 2022

How to submit

Submit your proposal to manuscripts@sciencesocieties.org

Please contact Jerry Hatfield at jerryhatfield67@gmail.com with any questions.

American Society of Agronomy | Crop Science Society of America | Soil Science Society of America

Received: 21 December 2021 | Accepted: 11 April 2022

DOI: 10.1002/agj2.21090

Agronomy Journal

ARTICLE

Agronomy, Soils, and Environmental Quality

Adapting the CROPGRO-faba bean model to simulate the growth and development of *Amaranthus* species

Peteh Mehdi Nkebiwe[1,2] | **Ken Boote**[3] | **Annegret Pflugfelder**[1,4] | **Sebastian Munz**[1] | **Simone Graeff-Hönninger**[1]

[1]Cropping Systems and Modelling (340 AG), Institute of Crop Science, Univ. of Hohenheim, Stuttgart 70599, Germany

[2]Current address: Fertilization and Soil Matter Dynamics (340 i), Institute of Crop Science, Univ. of Hohenheim, Stuttgart 70599, Germany

[3]Agricultural and Biological Engineering Dep., Univ. of Florida, Gainesville, FL 32611, USA

[4]Current address: Center for Organic Farming (309), Univ. of Hohenheim, Stuttgart 70599, Germany

Correspondence
Peteh Mehdi Nkebiwe, Cropping Systems and Modelling (340 AG), Institute of Crop Science, Univ. of Hohenheim, Stuttgart, Germany, 70599.
Email: mehdi.nkebiwe@uni-hohenheim.de

Assigned to Associate Editor Stephen Del Grosso.

Funding information
German Federal Ministry for Economic Affairs and Energy within the Central Innovation Program for SMEs (ZIM), Grant/Award Number: 16KN050528

Abstract

The aim of this study was to adapt the CROPGRO model to simulate growth and development processes of *Amaranthus* spp. under central European conditions. In 2017 and 2018, two field experiments with two amaranth cultivars (grain type, *A. hypochondriacus* L. Neuer Typ [NT]; fodder type, *A. caudatus* L. K63 [K63]) were conducted in southern Germany. Based on experimental and literature data, parameter coefficients that drive physiological processes at species, cultivar, and ecotype levels were calibrated to predict the time series experimental observations of various growth and development traits. Statistical evaluation of the model adaptation was performed using root mean square error (RMSE, in variable units, 0 equals perfect fit) and the Willmott agreement index (d-Stat., range from 0 to 1, 1 equals perfect fit). For NT and K63, respectively, the model adaptation led to accurate predictions of canopy height (RMSE, 0.07 and 0.24 m; d-Stat.,0.98 and 0.92), panicle weight (RMSE, 2,034 and 1,153 kg ha^{-1}; d-Stat., 0.92 and 0.94), panicle harvest index (RMSE, 0.05 and 0.06; d-Stat., 0.99 and 0.96), leaf N concentration (RMSE, 0.38 and 0.40%; d-Stat., 0.94 and 0.92) and aboveground biomass (RMSE, 2,948 and 2,572 kg ha^{-1}; d-Stat., 0.88 and 0.91). In summary, the CROPGRO model was successfully adapted for *Amaranthus* spp. The adapted model can be further improved as it is made available for evaluation in different locations and environments including limited soil N supply.

1 | INTRODUCTION

The use of mechanistic crop growth models by the scientific community to improve understanding of the interaction of crop genotype, environment, and management strategy at the level of physiological processes has increased substantially in recent decades (Jones et al., 2017). While crop models can be used to hypothesize genetic improvements to existing crop species and cultivars, they are also valuable tools to evaluate crop management strategies (Boote et al., 2002). They are useful instruments for assessing the functioning of cropping systems and predicting agronomic productivity under

Abbreviations: CUL, cultivar file; DAS, days after sowing; DM, dry matter; DSSAT, Decision Support System for Agrotechnology Transfer; ECO, ecotype file; K63, *Amaranthus caudatus* L. K63; LAI, leaf area index; NT, *Amaranthus hypochondriacus* L. Neuer Typ; SPE, species file.

defined environmental conditions such as probable climate change scenarios (Hoogenboom et al., 2021). CROPGRO is a generic crop model that is incorporated in the Decision Support System for Agrotechnology Transfer (DSSAT) suite of crop models (Hoogenboom et al., 2019; Jones et al., 2003). It is developed to use the same common FORTRAN code to simulate growth and development processes in different grain legumes (Boote et al., 2002). This feature makes CROPGRO known for its robustness and versatility (Boote et al., 2002; Di Paola et al., 2016) because it can be adapted to new crops or cultivars through modifications in the input files that determine species (.SPE file), cultivar (.CUL file), and ecotype (.ECO file) traits without requiring a change in the core FORTRAN code.

CROPGRO was originally developed to model soybean [*Glycine max* (L.) Merr.] (Boote, Jones, & Hoogenbom, 1998; Boote, Jones, Hoogenbom, & Pickering, 1998) and has been subsequently adapted for faba bean (*Vicia faba* L.), peanut (*Arachis hypogaea* L.), tomato (*Lycopersicon esculentum* Mill.), white cabbage (*Brassica* spp.), safflower (*Carthamus tinctorius* L.), chia (*Salvia* spp.), and quinoa (*Chenopodium quinoa* Willd.) (Boote et al., 2002; Boote, Jones & Hoogenboom, 1998; Mack et al., 2020; Präger et al., 2019; Scholberg et al., 1997; Singh et al., 2016; Steberl et al., 2020; Übelhör et al., 2015) among others. In so doing, assessments have also been made regarding the agronomic performance of new or exotic crop species that have been bred and adapted to grow in new geo-climatic environments (Mack et al., 2020; Präger et al., 2019).

In Europe, grain amaranth (*Amaranthus* spp.) is an exotic crop that is gaining importance in terms of consumer acceptance and growing imports as a niche cereal (CBI, 2021). Grain amaranth, a so-called "superfood," is a dicotyledonous C4 gluten-free pseudo-cereal that originates from Central and South America and is regarded as one of the world's oldest crops (Soriano-García & Aguirre-Díaz, 2019). *Amaranthus caudatus* L. is described as a non-obligate short-day plant (Zabka, 1961) and most *Amaranthus* spp. typically exhibit indeterminate growth where flowering, grain development, and maturation occur simultaneously with vegetative growth (Pandey & Singh, 2009). Grain amaranth is increasingly consumed in Europe because it is gluten-free, which makes it attractive for people with coeliac disease (CBI, 2021). Additionally, grain amaranth has high concentrations of various essential nutrients. In comparison to whole grain wheat (*Triticum aestivum* L.) for example, grain amaranth is richer in protein; fat; oleic fatty acid; Ca; Mg; Zn; Fe; and the essential amino acids lysine, threonine, and tryptophan (Alvarez-Jubete et al., 2009, 2010; Caselato-Sousa & Amaya-Farfán, 2012; Venskutonis & Kraujalis, 2013). Apart from the use of amaranth for human nutrition as a valuable grain or the leaves as a vegetable crop (Alvarez-Jubete et al., 2009, 2010; Caselato-Sousa & Amaya-Farfán, 2012; Chang et al., 2021; Sarker et al., 2018; Venskutonis & Kraujalis, 2013), it is also an important forage and fodder crop for cattle and pigs (Bora, 2018).

Core Ideas

- A physiological process-based mechanistic model was adapted to *Amaranthus* ssp. for the first time.
- Panicle weight and harvest index, leaf N concentration, and aboveground biomass were accurately predicted.
- *Amaranthus* spp. showed a low requirement for N and considerable drought tolerance.

Although a few grain amaranth cultivars have been adapted to grow under central European conditions (Gimplinger et al., 2007), most of the amaranth consumed in Europe is imported (CBI, 2021). The growing market value for grain amaranth also provides European farmers with an opportunity to diversify their cropping systems by including amaranth as an additional cash crop. The relatively moderate N requirement (Myers, 1998) and considerable drought tolerance (Alemayehu et al., 2015; Jacobsen et al., 2003) of *Amaranthus* spp. makes it particularly appealing to be included in central European cropping systems to improve resilience to the increasingly frequent drought events related to climate change (Spinoni et al., 2018).

The aim of this study was to (a) investigate and document the growth and development of selected grain and fodder *Amaranthus* spp. cultivars under the environmental conditions in southern Germany and (b) to use the resulting experimental data as well as published literature data to adapt the CROPGRO model to simulate the growth and development processes of the selected amaranth cultivars. Although CROPGRO was originally developed for soybean, which has pods holding large seeds, in this study, amaranth panicles are considered to be nonleaf and nongrain structures that are equivalent to pods and hold tiny seeds. Consequently, like pods, panicles also have relatively high lignin but low lipid, protein, and carbohydrate contents.

2 | MATERIALS AND METHODS

2.1 | Plant material

Two *Amaranthus* spp. cultivars that are adapted to central European long-day conditions were chosen for the field experiments. These cultivars were also selected because of their contrasting physical growth characteristics and different end uses (Table 1, Figure 1). *Amaranthus hypochondriacus* L.

TABLE 1 Characteristics and origin of *Amaranthus* spp. cultivars

Species	Cultivar	Physical characteristics	Origin
A. hypochondriacus L.	Neuer Typ (NT)	≈1 m tall, green stem and leaves, develops side-stems with panicles, main- (apical inflorescence) and side-stem (axillary inflorescence) panicles are green to pale-yellow in color, pale-yellow to white grains	Zeno Projekte[a]
A. caudatus L.	K63 (K63)	1.5–2 m tall, green to purple stem and leaves, small side-stems carrying panicles that rarely mature, purple to red panicle, dark-brown to black grains	Ihinger Hof[b]

[a]Zeno Projekte, Gentzgasse 129/1/10, 1180 Vienna, Austria.
[b]Seed material from earlier trials at Ihinger Hof, a research station of the University of Hohenheim, 71272 Renningen, Germany.

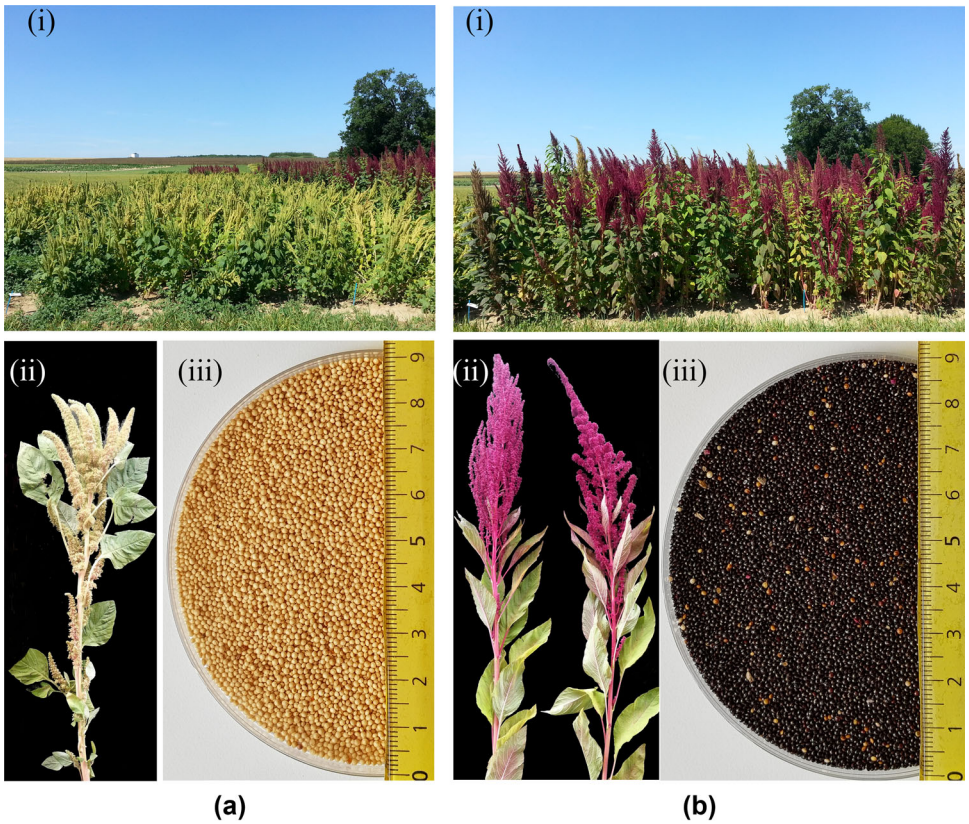

FIGURE 1 Physical characteristics of (a) *Amaranthus hypochondriacus* L. var Neuer Typ (NT) and (b) *A. caudatus* L. var K63 (K63). (a) Plot at experimental site (i), (b) shoot showing a main panicle (apical inflorescence), (c) grain

Neuer Typ (NT) is a typical grain amaranth cultivar because of its relatively large, pale-yellow to white, and starch-rich grains (thousand grain weight, TGW, 0.9 g; 60% starch), which makes them suitable for popping, and also because of its high harvest index (0.38) (Gimplinger & Kaul, 2009; Mlosch, 2015). Contrastingly, *A. caudatus* L. K63 (K63) is a typical fodder and forage amaranth cultivar that produces small, dark-brown to black grains (TGW ca. 0.6 g) that have a low starch content (49% starch) and are thus unsuitable for popping (Mlosch, 2015). K63 also produces much above-ground biomass and has a relatively lower harvest index in comparison to NT.

2.2 | Site characteristics

In 2017 and 2018, field experiments were conducted at two field sites at Ihinger Hof (48°44′ N, 8°55′ E, 478 m asl, Renningen, Germany), a research station of the University of Hohenheim (Stuttgart, Germany). The mean annual temperature of the site is 8.1 °C, the average annual rainfall is 690 mm, and the mean solar radiation is 11.4 MJ m^{-2} d^{-1} (Übelhör et al., 2015). The physical and chemical properties of the soils that can be characterized as haplic (2017) and vertic Cambisol (2018) (IUSS Working Group WRB, 2007) are given in Table 2. In both years, the previous crop was triticale

TABLE 2 Physico-chemical soil properties at the experimental sites

Depth	Bulk density	Clay	Sand	Silt	N_{min}	N_t	C_{org}
cm	g cm^{-3}	%			kg N ha^{-1}	%	
2017							
0–30	–	33.9	2.0	64.1	23.5	0.16	1.13
30–60	1.4	34.9	2.3	62.8	14.8	0.12	0.79
60–90	–	34.1	4.1	61.7	37.1	0.08	0.53
2018							
0–30	–	33.9	13.9	52.3	23.5	0.14	1.14
30–60	1.4	–	–	–	9.2	0.08	0.48
60–90	–	–	–	–	7.9	0.04	0.88

Note. $N_{min,}$ mineral nitrogen; N_t, total nitrogen; C_{org}, organic carbon.

TABLE 3 Monthly mean (T_{mean}), maximum (T_{max}), and minimum (T_{min}) daily temperatures, mean solar radiation, and cumulative rainfall at the experimental sites in 2017 and 2018

Month	T_{mean}	T_{max}	T_{min}	Solar radiation	Rainfall
	°C			MJ m^{-2} d^{-1}	mm
2017					
May	13.6	30.4	–0.1	18.9	47.0
June	18.3	32.0	5.2	23.5	72.2
July	18.2	31.7	9.0	18.1	109.9
Aug.	18.1	29.7	7.0	16.2	69.3
Sept.	11.8	23.5	2.3	11.3	52.2
Oct.	10.3	24.0	–2.3	8.2	51.1
2018					
May	14.9	26.9	2.6	18.9	75.1[a]
June	17.4	28.0	4.3	21.3	32.5
July	19.9	32.9	9.0	21.6	32.0
Aug.	19.6	33.6	4.2	17.4	28.8
Sept.	14.8	28.6	–0.3	14.9	78.0
Oct.	10.1	24.4	–1.5	10.9	26.4

[a]Severe storm on 31 May 2018 with 34.7 mm rainfall within 1 h.

(× *Triticosecale* Wittmack). In 2017, 1 t of straw ha^{-1} was retained onsite and plowed to about 25-cm depth whereas in 2018, 5 t ha^{-1} were plowed to the same depth.

According to an on-site weather station, the mean annual temperature and rainfall across the years 2012–2019 were 9.6 °C and 671.9 mm, respectively. The monthly mean, maximum, and minimum daily temperatures; mean solar radiation; and cumulative rainfall for 2017 and 2018 are given in Table 3.

2.3 | Field experiments

In both years, the experiments were arranged in a randomized complete block design (RCBD) with three replicates. The factors included: (a) two amaranth cultivars (NT and K63) and (b) three N-fertilizer levels (0, 50, and 75 kg N ha^{-1}) applied as calcium ammonium nitrate after accounting for the 2017 soil mineral nitrogen content (N_{min}). Although a lower soil N_{min} content was reported in 2018 (Table 2), the same N-fertilizer levels as in 2017 were maintained for the purpose of consistency. The same plot size (60 m^2, 10 m by 6 m), row spacing (33 cm, 16 rows $plot^{-1}$), sowing depth (ca. 1 cm), and sowing density (230 seeds m^{-2}) were maintained in both years.

On 12 May 2017, 50 kg N ha^{-1} was broadcasted and incorporated (4-to- 5-cm depth, Fendt 207 Tractor, AGCO GmbH; UKS 150 Rauch Fertilizer spreader, RAUCH Landmaschinenfabrik GmbH) in plots belonging to the second N level (50 kg N ha^{-1}) whereas 37.5 kg N ha^{-1} (50%) was applied in plots in the third N level (75 kg N ha^{-1}) using the same

method. After fertilizer application on the same day, all plots were sown (Fendt 207 Tractor, AGCO GmbH). For the plots in the third N level (75 kg N ha^{-1}), the remaining 35.5 kg N ha^{-1} (50%) was top-dressed on 9 June 2017.

In 2018, the plots were fertilized (broadcast and incorporation) and sown on 25 May 2018. However, due to a severe storm on 31 May 2018 (34.7 mm rainfall within 1 h) that led to the erosion of surface soil leading to severe crusting, poor and heterogenous germination, the experiment was terminated on 18 June 2018 by chisel plowing all plots to a depth of 4–5 cm. The plots were then resown on 19 June 2018. The plots in the third N level were top-dressed with 37.5 kg N ha^{-1} on 19 July 2018. There was a severe drought in June and July 2018, which made irrigation necessary. Using a sprinkler system, the plots were irrigated on the following dates: 22 June (3 mm), 25 June (5 mm), 29 June (9 mm), 2 July (6 mm), 3 July (6 mm), 11 July (6 mm), 18 July (3 mm), 19 July (6 mm), 26 July (6 mm), 31 July (6 mm), 3 August (3 mm), 6 August (3 mm) and 7 August (3 mm). The total amount of irrigation was 65 mm.

When necessary, weed control was done mechanically between the rows during the early growth stage and manually between and within the rows at later growth stages. Insecticide treatment was performed when required. Whereas nondestructive data and destructive sample collection were performed on one-half of each plot, the other half was reserved for the final harvest. Each plot half was made up of four central plant rows that were relevant for sampling and data collection while two unsampled border rows were maintained on each side.

2.4 | Data collection

Phenological development stages from emergence to maturity were recorded weekly on the basis of the BBCH scale (Meier et al., 2009), which has also been subsequently established for amaranth (Martínez-Núñez et al., 2019). The occurrence date for the following important growth stages were recorded: emergence (cotyledons fully emerged), first pair of true leaves visible, emergence of apical inflorescence (main-stem panicle), start of anthesis on main-stem panicle (extrusion of anthers), seed set (first seeds) and maturity (ripe seeds). Due to the indeterminate growth of *Amaranthus* spp. (Pandey & Singh, 2009), it proved challenging to accurately record the start of anthesis because extruded anthers quickly senesced and were shed off the panicle. Similarly, the start of maturity was also challenging to accurately ascertain due to shedding of grain that matured early, which also occurred parallel to flowering (anthesis, starting on the upper half of the main panicle) and seed development.

For the nondestructive data collection, five consecutive representative plants were identified and marked in the central area of each plot. Data were collected on a weekly basis between 33 and 110 days after sowing (DAS) in 2017 and 37 and 92 DAS in 2018. Data were collected on the following growth traits: total number of leaves on the main stem (also nodes), number of senescent or missing leaves on the central axis, canopy height, canopy width (perpendicular to the row), emergence of an apical inflorescence (main-stem panicle) or axillary inflorescences (side stem panicles) and flowering date. When conditions were favorable, photosynthetically active radiation (PAR) interception by the canopy at noon was measured (AccuPAR, PAR/LAI Ceptometer, Model LP-80, Decagon Devices, Inc.). In 2018 (59–64 DAS), the rate of photosynthesis on the youngest fully expanded leaf was measured around noon under field conditions as a function of increasing intensity of artificial light (13 intensities from 0 to 2,000 μmol m^{-2} s^{-1}; reference CO_2 concentration, 380 μl L^{-1}) (LCpro-SD System, Serial No.33433, ADC BioScientific LTD, Herts EN11 0NT, UK). Due to time and labor constraints, only plots supplied with 75 kg N ha^{-1} were considered for the measurement of photosynthesis rates on two plants per replicate for NT and one plant per replicate for K63.

Destructive sampling was done on a biweekly basis starting on 45 DAS (2017) and 37 DAS (2018), and ending on 116 DAS (2017) and 94 DAS (2018). Sampling was done in the central four rows of the area assigned for the destructive samplings. Each sampling comprised an area of 0.264 m^2 (0.2 by 1.32 m). The sampling position for each date was randomly assigned before the experiment. Between sampling positions a border of 0.5 m was kept. Data on the following traits were collected: number of plants, total fresh aboveground biomass, and for two selected representative plants: height, width, number leaves on the main stem number of leaves on the side branches, total leaf area (nonsenescent leaves on the main stem and side branches measured with LI-3100 Area Meter, LI-COR), fresh (FM) and dry matter (DM) content (70 °C until constant weight) of leaves, stems (stem plus leaf petioles), panicles, or threshed panicles (if grains were ripe enough to enable threshing), and grain. Specific leaf area (SLA, cm^2 g^{-1} leaf DM) was calculated based on leaf area and leaf DM. Mean aboveground biomass DM concentration of the two representative plants was used along with total fresh biomass to determine the total shoot DM of the sampling area (0.264 m^2). Using the mean partitioning coefficients of total aboveground biomass DM to various organs, the leaf DM in the sampling area was determined. Leaf area index (LAI) was determined as follows:

$$\mathrm{LAI} = \frac{\text{Leaf DM in sampling area (g)}}{\text{Sampling area } \left(0.264\ \mathrm{m}^2\right)} \left[\text{mean SLA}\left(\frac{\mathrm{cm}^2}{\mathrm{g}}\right)\right] \frac{1\ \mathrm{m}^2}{10{,}000\ \mathrm{cm}^2} \quad (1)$$

As for other traits, amaranth panicles (inflorescences) were morphologically diverse. Intraspecific polymorphism in amaranth is linked to incomplete domestication (Stetter et al., 2017; Stetter et al., 2019). For consistency, total panicle biomass was defined as both the terminal panicle (apical inflorescence) on the main stem, cut above the youngest leaf, and the axial panicles (axillary inflorescence) on the side stems, also cut above the youngest leaf on the side stem. If present, single panicles branching out below the youngest leaf on the main or side stem were excised at the node and included within the panicle biomass.

Thousand grain weight was determined using a seed counter (Contador seed counter, Pfeuer GmbH). Absolute grain dry weight was determined after drying at 105 ˚C for 24 h. The N concentration in the dried and ground leaf, stem, panicle, and grain tissue was determined (vario Macro cube Elementar Analyzer, Elementar Analysesysteme GmbH). Grain crude protein content was calculated by multiplying the N concentration by the factor 6.25 (AOAC, 1990).

Final harvest was done manually on 133 DAS (2017) and 106 DAS (2018) in order to reduce grain loss from shattering, which can be made worse by the vibrations of a mechanical harvester. The designated manual harvest area was the four central rows (1.32 m) to a length of 2.2 m in 2017 (2.9 m^2) and three central rows (0.99 m) to a length of 2.0 m in 2018 (1.98 m^2). The remaining plot was harvested mechanically with a plot combine harvester (Zürn 170, Zürn Harvesting GmbH & Co. KG).

2.5 | Modelling methodology

To adapt the CROPGRO model to simulate growth and development processes in *Amaranthus* spp., parameters considered to be genetic coefficients in various files were modified and adapted based on values that were: (a) calculated/estimated from our experimental data; (b) reported in published scientific literature; or (c) assumed for the best fit of simulations to observations, where our experimental data or literature data was not available. Although the cardinal temperatures for *Amaranthus* spp. (warm-season C4 crops) are, generally speaking, higher than those for legumes like faba bean or soybean (which are relatively cool-tolerant temperate crops), the CROPGRO legume model was chosen as a starting point for the model adaptation because amaranth is also a cool-tolerant temperate crop. Furthermore, amaranth is a pseudo-cereal and its growth and development characteristics are more closely related to those of legumes than to those of typical cereals like maize (*Zea mays* L.) or wheat. Instead of the CROPGRO soybean model, the CROPGRO Faba bean model template (*.SPE, *.ECO, and *.CUL) was chosen because *Amaranthus* spp. produces a high amount of aboveground biomass, which makes it more comparable to faba been than to soybean in this context. Further, prior experience with the adaptation of the CROPGRO legume model to other crops was an additional advantage.

All the required input files for the model adaptation were created and entered into DSSAT V4.7 (Hoogenboom et al., 2019). These included the: (a) species (.SPE), cultivar (.CUL), and ecotype (.ECO) files, which provide genetic coefficients for various growth and development traits. To create these files, FBGRO047.SPE, FBGRO047.CUL, and FBGRO047.ECO in DSSAT Version 4.7 were used as the starting point (template). Initially, the photoperiod function indicating photoperiod sensitivity at growth phases was turned off (.SPE) and the critical short daylength (CSDL) and the slope of photoperiod sensitivity (PPSEN) for generic faba bean (Almeda) were assumed to be correct (.CUL). (b) The weather file (.WTH), which contained daily maximum and minimum temperatures, daily solar radiation, and daily rainfall. (c) The soil file (.SOL) that was created using the SBuild program in DSSAT V4.7 and provided coefficients to soil parameters such as soil albedo, evaporation limit, drainage rate, and different soil base layer depths and their respective properties: bulk density, pH, organic C, and N contents, drained upper and lower limits, texture and root growth factor. (d) The X file (.FBX) was created using the XBuild program in DSSAT V4.7 and this provided information about experimental conditions: environment and soil conditions, management, treatments, and simulation options. The Priestley–Tylor/Ritchie option for evapotranspiration was used. Symbiotic N_2 fixation was turned off because *Amaranthus* spp. are not legumes. Nitrogen balance was initially turned off and water balance was turned on. (e) Experimental data were entered into the T file (.FBT, for time-course data) and the A file (.FBA, average performance and final harvest) to enable comparison between simulations and actual experimental observations.

The systematic approach for model calibration described by Boote (Boote, 1999; Boote et al., 2002) was adopted. It included the following steps: (a) Values from literature or our experimental observation were obtained for: cardinal temperatures (T_b, $T_{opt}1$, $T_{opt}2$, and T_{max}); composition of protein, carbohydrate, lipid, lignin, organic acid, and mineral in different plant tissues; and critical leaf N concentration for photosynthesis for various growth and development processes. (b) Using real weather data provided in .WTH file, the threshold values of photothermal days (PD) were adjusted in the .CUL and .ECO files to predict the observed crop life cycle and development stages: PL-EM (planting to emergence), EM-V1 (emergence to first true leaf), EM-FL (emergence to anthesis), and SD-PM (first seed to maturity). Different EM-FL values were also used to differentiate between the development rates of NT and K63. (c) Simulations of time-series growth variables were made, and parameters modified with the target to approach similar values over time with low RMSE and high d-Stat (see section 2.6. Statistical

Evaluation). The canopy height and width growth parameters (XVSHT, YVSHT, and YVSWH) in the .SPE file, the leaf appearance rate parameter (TRIFL) and relative height and width parameters (RHGHT, RWIDTH) in the .ECO file were also modified based on measured height, width, and leaf number (on the main stem) of each cultivar to correctly and differentially predict the plant height, width, and leaf number for NT and K63. (d) Simulated specific leaf area (SLA), leaf area index (LAI), and aboveground biomass were compared with observed time series experimental data and the parameter(s) determining standard reference SLA at early vegetative stage (SLAREF), SLA of cultivars under standard growth conditions (SLAVR, value is close to SLAREF), the sensitivity of SLA to low and high light intensity respectively (SLAMAX and SLAMIN), maximum photosynthesis rate (LFMAX, from our field measurements), and early sink-limited leaf area expansion (SIZREF) and maximum leaf area (SIZLF) were adjusted in the .SPE and .CUL files. The modification of LFMAX was based on measured light saturated photosynthesis on the field. (e) After readjusting for the best fit of aboveground biomass predictions to experimental observations, XFRT, the parameter that describes the fractional partitioning of photosynthates to the panicles including seeds in the .CUL file was adjusted to achieve best fit between simulated and observed time-series panicle weight and panicle harvest index. Different values of XFRT were also required to differentiate between NT and K63. The parameters driving the time between first flower and end of leaf expansion (FL-LF), and the fraction of DM growth allocated to stem (FRSTMF) and leaf (FRLFF) at the end of leaf expansion were adjusted for best fit of simulated and observed stem and leaf weights. (f) Small adjustment in the parameter SLWREF (Specific leaf weight at which LFMAX is defined) was made to re-fit the overall productivity. Minor modifications in FL-SH (photothermal days (PD) between first flower and panicle appearance), FL-SD (PD between first flower and first seed), and FL-VS (PD from first flower to last leaf on the main stem) were made to fit the observed life cycle. (g) To mitigate drought stress problems related to water uptake in 2018, the root growth parameters XRTFAC and YRTFAC (maximum root length progression per physiological day), RTDEPI (initial root depth at emergence), and SRGF (root growth in soil layers, .SOL) were adjusted to reduce drought stress effects and to best fit the predicted productivity to observed values. (h) Vegetative partitioning parameters (YLEAF and YSTEM as a function of XLEAF, main stem node number) were adjusted to fit the predicted leaf and stem biomass to the observed values. Carbon (NMOBMX) and nitrogen (NVSMOB) mining parameters, and leaf senescence factors (SENRTE and SENRT2) were adjusted to regulate the remobilization of N and C from vegetative to reproductive tissues. These were adjusted for the best fit of the simulated N concentrations in leaf, stem and shell (panicle minus grains) tissues to the observed time series values. (i) To calibrate the initial seed weight, seeds per panicle, and the duration of pod addition and seed filling, the parameters determining maximum weight per seed (WTPSD), average seed per pod (SDPDV), seed filling duration (SFDUR), pod addition duration (PODUR), photothermal duration between first seed and physiological maturity (SD-PM) and the cut-off point for last seed addition within SD-PM (PMO9) were adjusted and differentiated for NT and K63. (j) Going through steps b to h, small adjustments were made to TRIFL, SIZLF, and XFRT, and the sensitivity of leaf expansion to low temperatures was increased by adjusting the values in the parameters XSLATM and YSLATM. (k) The maximum ratio of grain to panicle (grain plus shell) at maturity (shelling %) was adjusted for NT and K63 by modifying the parameter THRSH to achieve best fit between predicted and observed data. Final leaf and stem weights were recalibrated for best fit by slightly adjusting PORPT, which determines the loss of leaf plus leaf petiole with senescence, SENRTE and XFRT.

2.6 | Statistical evaluation

The evaluation of the fit between simulated and experimental time-course data was done visually and by inspection of improvements in the statistical indices after parameter modification steps above: (a) root mean square error (RMSE); (b) and the Willmott agreement index (d-Stat.) (Willmott, 1982). The RMSE is in the unit of the variable in question and a value of 0 represents a perfect fit, whereas the value of d-Stat. ranges from 0 to 1, with 1 indicating a perfect fit. Both indices are given by the formulae below:

$$\mathrm{RMSE} = \sqrt{\sum_{i=1}^{n} \frac{\left(S_i - O_i\right)^2}{n}} \tag{2}$$

$$d - \mathrm{Stat.} = 1 - \frac{\sum_{i=1}^{n} \left(O_i - S_i\right)^2}{\sum_{i=1}^{n} \left[\left(S_i - \bar{O}\right) + \left(O_i - \bar{O}\right)\right]^2} \tag{3}$$

where n is the number of samples, S_i is the simulated, and O_i the observed experimental value for the ith observation, and $\bar{O}$ is the mean of the observed values.

3 | RESULTS AND DISCUSSION

3.1 | Model adaptation

3.1.1 | Drought stress and seed size

As reported earlier, drought stress-related simulation issues in 2018 were mitigated by modifications in the parameters that drive root growth in both the .SPE and .SOL files to

improve water acquisition from deeper soil layers. The soil layers were increased in increments of 30 cm to a depth of 180 cm and the initial volumetric water content was set at field capacity (0.406 cm^3 cm^{-3}). Additionally, the method for the quantification of soil evaporation was changed from "Suleiman-Ritchie" to "Ritchie-Ceres," which limits evaporation to the top soil layer, thus, allowing the bottom soil layers to not be depleted by soil evaporation and increasing the quantity of plant-available water.

The single seed weight NT and K63 of 0.0008 g (0.0006–0.001 g) is several times smaller than the minimum seed weight 0.06 g allowed by CROPGRO. To solve this issue, WTSPSD was set at 0.08, which was a hundred times the actual seed weight of 0.0008 g. Consequently, the number of grains per m^2 were reduced accordingly by a factor of 100 to correct for the change.

Soil N_{min} (0–90 cm) was 75.4 kg N ha^{-1} and 40.6 kg N ha^{-1} in 2017 and 2018, respectively (Table 2). Despite the differences in soil N_{min} and N-fertilizer treatments (0, 50, and 75 kg N ha^{-1}), a repeated measures linear regression of the effect of N-fertilizer level and year on the weight of various plant organs and on LAI revealed that N fertilizer level mostly had no significant effect. It showed that the crop N requirement was covered by the moderate-to-high initial soil N_{min} levels in both years as well as by N released from the mineralization of the incorporated residues from the previous crops. This confirms that amaranth has a moderate requirement for N (Myers, 1998). As a test, N balance was turned on in the .FBX file and the fit of simulated to observed data across all measured traits was compared with the fit when N balance was turned off. This comparison showed that RMSE and d-Stat. were not improved with N balance turned on. Therefore, N balance was turned and kept off during the rest of the calibration process.

During the 2018 cropping season (May–October), there was less rainfall (272.8 mm rainfall, +65 mm irrigation) and higher mean daily temperatures (16.12 ˚C) than in 2017 (401.7 mm, 15.1 ˚C). Due to the considerable differences in the environmental conditions (soil N_{min}, temperature, rainfall) between both trial years, it was decided to use the observed time-series data from both site-years for the model adaptation process. The use of data from contrasting environments for model calibration can substantially improve the robustness of the calibrated model (He et al., 2017). Nevertheless, the true robustness of our model will depend on evaluation in other environments and locations.

3.1.2 | Temperature effects on growth and development

The cardinal temperatures that drive various growth and development processes were set based on values reported in literature or assumed. These are given in Table 4. The minimum germination temperature of some amaranth species is around 5 ˚C, whereas the optimal germination temperature is said to range from 25 to 40 ˚C (Assad et al., 2017). For the germination of *A. retroflexus* L., the base temperature (T_b) of 7–12 ˚C, optimal temperature ($T_{opt}1$ – $T_{opt}2$) of 35–40 ˚C and maximum temperature (T_{max}) of 40 ˚C have been reported (Krähmer, 2016). The T_b for the vegetative development was set to 7 ˚C (Bello & Walker, 2017; Nyathi et al., 2018) and the T_b of early (flowering to first seed) and late (first seed to maturity) reproductive processes was set at 8 ˚C (Gimplinger & Kaul, 2009). The $T_{opt}1$, $T_{opt}2$, and T_{max} for the vegetative and both early and late reproductive processes were 30 ˚C (Bello & Walker, 2017), 35 ˚C (assumed), and 40 ˚C (Assad et al., 2017; Nyathi et al., 2018), respectively. Values of 30 and 40 ˚C have both been used as the upper temperature for modelling blood amaranth (*A. cruentus* L.) (Bello & Walker, 2017; Nyathi et al., 2018). This suggests that a T_{max} of 40 ˚C may be a rather conservative value for growth. The T_b, $T_{opt}1$, $T_{opt}2$, and T_{max} for light saturated photosynthesis were set to 7, 40, 44, and 48 ˚C respectively. This value for T_{max} is comparable to values reported for *A. edulis* Speg. (*A. caudatus*) (50–55 ˚C), which was grown under various CO_2 levels (El-Sharkawy et al., 1968). Due to lack of published data, the effect of temperature on leaf expansion, pod set, and seed growth rate were assumed by slightly increasing the default values for faba bean.

3.1.3 | Tissue composition and nutrient mobilization

The maximum or initial composition of protein; carbohydrate; lipid; lignin; organic acid; and mineral in leaf, stem, root, shell (panicle without seed) and seed tissues were obtained from our experimental data, from published literature or assumed for best fit (Supplemental Table S1). For lignin, organic acid and mineral composition, the default values in the CROPGRO-Faba bean model were mostly maintained due to absence of information in literature. Seed protein (SDPROS) and lipid (PLIPSD) composition are cultivar parameters given in the .CUL file under the abbreviations SDPRO and SDLIP, respectively (Supplemental Table S1). For leaf protein composition, a typical value for normal growth and a minimal value at the end of growth (onset of senescence), which are both required by CROPGRO, were set at 0.24 and 0.09, respectively. The parameters CMOBMX (maximum fractional daily mobilization rate of carbohydrates from vegetative tissues), NMOBMX (maximum fractional mobilization of protein from vegetative tissues during reproductive growth), NVSMOB (mobilization of protein during vegetative growth, 0–1 scaled on NMOBMX) were set at 0.026, 0.16, and 0.45, respectively, to enable mobilization of leaf N to

TABLE 4 Cardinal temperatures and functions used by the CROPGRO model for growth and development processes of amaranth, compared with template default values for faba bean

Process	Shape	Default temperatures,faba bean				Modified temperatures, *Amaranthus*			
		T_{base}	$T_{opt}1$	$T_{opt}2$	T_{max}	T_{base}	$T_{opt}1$	$T_{opt}2$	T_{max}
		°C							
Vegetative development, node expression rate	Lin.	0	27	30	40	7	30	35	40
Early reproductive development, flowering to first seed	Lin.	0	22	26	45	8	30	35	40
Late reproductive development, first seed to maturity	Lin.	0	22	35	45	8	30	35	40
Light-saturated leaf photosynthesis, LF_{max} vs. current temperature	Lin.	1	30	31	40	7	40	44[a]	48
Light-saturated leaf photosynthesis, LF_{max} vs. T_{min}	Qdr.	−2	14	–[b]	–[b]	−1	15	–[b]	–[b]
Leaf relative expansion, effect on SLA	Lin.	2[c]	20	–[b]	–[b]	4[c]	21[d]	–[b]	–[b]
Pod set, effect on pod addition and seed addition rate	Qdr.	6	15	24	34	7	21	24	34
Seed growth, effect on seed growth rate	Qdr.	2	18	21	36	3	20	21	36

Note. T_{base}, base temperature; $T_{opt}1$, first optimum temperature; $T_{opt}2$, second optimum temperature; T_{max}, maximum temperature; Lin., linear function; LF_{max}, maximum leaf photosynthetic rate; T_{min}, minimum temperature; Qdr., quadratic function; SLA, specific leaf area.

[a]Relative rate at $T_{opt}2$ is 0.8.

[b]Relative rate remains high above $T_{opt}1$.

[c]Relative rate at T_{base} is 0.25.

[d]Relative rate at $T_{opt}2$ is 0.35.

reproductive organs to achieve the target leaf N concentration at physiological maturity.

3.1.4 | Phenology

One of the early studies on *A. caudatus* concluded that it was distinctly a short-day plant (Fuller, 1949). In contrast, a later study showed that it is not an obligate short-day plant as previously described because flowering could still be induced under long-day conditions of 18 h even though the flowering date was delayed. In comparison to landraces, cultivated *Amaranthus* spp. and cultivars may have lost their photoperiod sensitivity to some degree through breeding, although most species show some sensitivity to daylength (Wu et al., 2000). Therefore, the photoperiod function, indicating presence or absence of photoperiod sensitivity during growth phases: (a) End of Juvenile (END JV) to Flower induction (FL IND); (b) Flower induction (FL IND) to First flower (1ST FL) was changed to NON (absent or off) in the species file (.SPE).

To fit the duration of simulated to observed development phases, various parameters related to genetic coefficients for crop development in the cultivar file (.CUL) were modified based on experimental observations, literature reports or assumed for best fit (Table 5). The CROPGRO parameters which determine the duration of various phases: the time in photothermal days (PD) between plant emergence and flower appearance (EM-FL), first flower and first pod (FL-SH), first flower and first seed (FL-SD), first seed and physiological maturity (SD-PM) and first flower and end of leaf expansion (FL-LF) were modified for best fit of simulated and observed crop life cycle (Table 5). As earlier indicated, it was difficult to accurately determine the start of anthesis because extruded anthers quickly senesced and were shed off the panicle. As described for the adaptation of CROPGRO to quinoa (Präger et al., 2019), similarly amaranth pods (panicles) appear before flowering; therefore, the anthesis date was set for accurate prediction of the start of seed set.

The maximum leaf photosynthetic rate (LFMAX defined at 30 ˚C, 350 µl L^{-1} CO_2, and high light) was set to 2.5 mg CO_2 m^{-2} s^{-1}, which corresponds to the field measurements at 59–64 DAS in 2018 on the youngest fully developed leaves of plants fertilized with 75 kg N ha^{-1}. Additional parameters were modified to adequately predict productivity; leaf, panicle, and seed weight; seed protein; and lipid content. These included: specific leaf area of cultivar under standard growth conditions, SLAVR (cm^2 g^{-1}); maximum size of full leaf, SIZLF (cm^2); maximum fraction of daily growth that is partitioned to seed and pod or panicles, XFRT; maximum weight per seed, WTPSD (g); seed-filling duration for pod cohort at standard growth conditions, SFDUR (photothermal days, PD); average seed per pod under standard growing conditions, SDPDV (No. pod $^{-1}$); duration of pod addition under

TABLE 5 Genetic coefficients in the cultivar file (.CUL) in the CROPGRO model and modifications used to calibrate processes in the *Amaranthus* cultivars Neuer Typ and K63

Parameter	Parameter abbreviation	Default, faba bean Almeda	*A. hypochondriacus* L. Neuer Typ	*A. caudatus* L. K63
Time between plant emergence and flower appearance, R1 (PD)	EM-FL	18	11.7	14.7
Time between first flower and first pod, R3 (PD)	FL-SH	10.9	3.5	3.5
Time between first flower and first seed, R5 (PD)	FL-SD	24	9.8	9.8
Time between first seed (R5) and physiological maturity (R7) (PD)	SD-PM	34.5	24.6	24.6
Time between first flower and end of leaf expansion (PD)	FL-LF	45	25.0	25.0
Maximum leaf photosynthetic rate at 30 ˚C, 350 μl L^{-1} CO_2, and high light, mg CO_2 m^{-2} s^{-1}	LFMAX	1	2.5	2.5
Specific leaf area of cultivar under standard growth conditions, cm^2 g^{-1}	SLAVR	285	230	210
Maximum size of full leaf, cm^2	SIZLF	110	33	32
Maximum fraction of daily growth that is partitioned to seed and shell	XFRT	1	0.89	0.62
Maximum weight per seed, g	WTPSD	1.1	0.08[a]	0.08[a]
Seed-filling duration for pod cohort at standard growth conditions (PD)	SFDUR	21	26	25
Average seed per pod under standard growing conditions, No. pod^{-1}	SDPDV	2.4	24	24
Duration of pod addition under standard conditions (PD)	PODUR	18	24	24
Maximum shelling percentage [seed × 100%/(seed + shell)] at maturity, %	THRSH	77	57	52
Fraction of protein in seeds, g protein $(g\ seed)^{-1}$	SDPRO	0.315	0.157	0.157
Fraction of oil in seeds, g oil $(g\ seed)^{-1}$	SDLIP	0.02	0.104	0.104

Note. PD, photothermal days.

[a]*Amaranthus* grain weight of 0.0008 g $seed^{-1}$ was increased by a factor of 100 to solve problems associated with the model code inability to simulate tiny seeds. The number of grains per m^2 were reduced accordingly by factor of 100 to correct for the change.

standard conditions, PODUR (PD); maximum shelling percentage [seed × 100%/(seed + shell)] at maturity, THRSH (%); fraction of protein in seeds, SDPRO [g protein $(g\ seed)^{-1}$]; and fraction of oil in seeds, SDLIP [g oil $(g\ seed)^{-1}$]. In addition, the following parameters were differentially modified to predict the differences between NT and K63: EM-FL, SLAVR, SIZLF, XFRT, SFDUR, and THRSH.

As part of the calibration process, parameters in the ecotype file (.ECO) were also modified to improve the prediction of the duration of life cycle phases, leaf appearance rate and plant height differentially for NT and K63. The parameters determining internode length (YVSHT) and canopy width (YVSWH) per node as a function of vegetative stage (XVSHT) in the species file (Supplemental Table S2) and those determining relative canopy height (RHGHT) and width (RWIDTH) in the ecotype file were modified to predict observed canopy height and width. The modified parameters are given for NT and K63, respectively: (a) Time between planting and emergence (PL-EM, in photothermal days [PD]): 2.5, 2.5; (b) Time required from emergence to first true leaf (EM-V1, PD): 1.3, 1.3; (c) Proportion of time between first seed and physiological maturity that the last seed can be formed (PM09): 0.65, 0.65; (d) Time from first flower to last leaf on the main stem (FL-VS, PD), 15.5, 22.5; v.) Rate of appearance of leaves on the main stem (TRIFL, Leaves PD^{-1}): 1.15, 1.10; (e) Relative height of an ecotype (RHGHT) in comparison to the standard height per node (YVSHT) defined in the species file (.SPE): 1.00, 1.25.

3.1.5 | Root and leaf growth, photosynthesis, partitioning, leaf senescence, canopy height and width

The model parameters in the CROPGRO species file (.SPE) that were modified from the faba bean default values to simulate growth and development processes in *Amaranthus* spp. are given in Supplemental Table S2. The initial rooting depth at emergence (cm) (RTDEPI) was reduced from 25 cm for

faba bean to 10 cm for *Amaranthus* spp. in accordance with field observations and the maximum rate of root depth progression (cm physiological day^{-1}) was increased. Amaranth is able to respond to drought stress by increasing its rooting depth (Johnson & Henderson, 2002). The later modification as well as the previously mentioned increase in the root growth factor in soil layers (SRGF, values from 0.0–1.0) in the soil file (.SOL) were made to minimize the simulated drought stress in 2018 to fit the predicted values to observed crop performance and biomass production. For the soil layer depths of 30, 60, 90, 120, 150, and 180 cm, SRGF was set to 1.0, 0.65, 0.50, 0.40, 0.30, and 0.20, respectively. This adjustment of SRGF values thus increased the depth of the potential rooting profile across soil layers. Furthermore, the maximum rate of rooting front depth progression (YRTFAC vs. XRTFAC) (cm physiological day^{-1}) in the .SPE file was increased from 2.6 for faba bean to 3.5 for *Amaranthus* spp. (Supplemental Table S2). This value is higher than 2.7 cm day^{-1} that has been used to simulate the growth of *A. cruentus* L. using the AquaCrop model (Bello & Walker, 2017), however in CROPGRO the resulting root growth is affected by temperature The adjustments on RTDEPI, YRTFAC vs. XRTFAC and SRGF led to a simulated rooting depth of 1.26 m at about 8 wk after emergence, which is in accordance with the depth of water extraction of 1.0–1.50 m soil zone at 8 wk after emergence that was observed for four grain amaranth cultivars grown in three successive growing seasons (Johnson & Henderson, 2002).

The parameters driving the effect of temperature on leaf-level photosynthesis in CROPGRO are given in Table 4. Other parameters in the CROPGRO species file (.SPE) that were modified to simulate growth and development processes in *Amaranthus* spp. are given in Supplemental Table S2. The quadratic (QDR) function that defines leaf photosynthesis response to leaf N concentration [FNPGN(4)] has a minimum of 0.68 and maximum of 2.93%. As a nonlegume, these values are appropriately lower than the corresponding values for the legume faba bean, and the 2.93% maximum is close to the 3.39% measured in the leaves used for field LFMAX measurements. SLWREF, the parameter for specific leaf weight at which LFMAX is defined was modified to account for the thinner leaves in *Amaranthus* spp. in comparison to faba bean.

The following parameters were modified to predict specific leaf area (SLA) and leaf area index: the SLA of leaves at plant emergence (FINREF); the SLA of the newly produced leaves in response to solar radiation (SLAMAX and SLAMIN) as well as response to a temperature function. In addition, the rate of leaf area expansion though the first VSSINK node number (5), during which leaf area expansion can be sink-limited, after which leaf area growth is totally source-driven by photosynthesis and partitioning of assimilate to leaf mass.

The prediction of canopy height and width was improved to fit experimental observations by adjusting the internode length per node (YVSHT) and canopy width per node (YVSWH) as a function of vegetative growth stage (VSTAGE). As indicated earlier, the relative heights (RHGHT) of the individual cultivars were differentiated from each other in the ecotype file (.ECO) NT and K63.

To improve the prediction of the dry weights of leaf and stem, the parameters for the partitioning of daily assimilate to leaf (YLEAF), stem (YSTEM), and root as a function of the vegetative stage (XLEAF) were modified. The fraction of vegetative dry matter allocated to stem (FRSTMF) and leaf (FRLFF) by the end of leaf expansion was adjusted to improve the prediction of leaf and stem biomass later in the life cycle. Leaf mass over time is also affected by leaf abscission as a function of node number (XSTAGE) and SENPOR during vegetative growth, while during grain-filling, leaf abscission is driven by the rate of N mobilization (NMOBMX) along with a parameter that specifies the grams of leaf mass lost per gram of protein mobilized (SENRTE). In addition, during that same process, a portion of biomass is lost from stem, which assumes that leaf petiole is also abscised (PORPT, as a fraction of leaf mass abscised). After physiological maturity, the rate of leaf abscission occurs as a function of calendar days (SENRT2).

3.2 | Goodness of fit of simulations to observations

3.2.1 | Leaf number, crop life cycle, and canopy height

Figure 2 illustrates the rate of main stem leaf appearance over time. The root mean square error (RMSE) of leaf number for NT and K63 were 4.2 and 6.1 and the Willmott agreement indices (d-Stat.) were 0.77 and 0.87, respectively. To achieve this, the base (T_{base}), first ($T_{opt}1$), and second optimum ($T_{opt}2$) temperatures of the linear function that determine leaf appearance rate were set at 7, 30, and 35 ˚C with values higher than faba bean, which shows the warm-season crop tendencies of *Amaranthus* spp. (Table 4). Likewise, the corresponding cardinal temperatures for rate of reproductive progress were set at 8, 30, and 35 ˚C, which are higher than faba bean and show *Amaranthus* warm-season crop tendencies. The default number of photothermal days (PD) required between planting and emergence (PL-EM) was set (Supplemental Table S2) to predict the observed emergence of *Amaranthus* spp. at 5 and 6 DAS in 2017 and 2018, respectively. To fit the simulated and observed leaf numbers on the main stem for each *Amaranthus* spp. cultivar, the photothermal time required between emergence and first true leaf (EM–V1) was reduced and the appearance rate of leaves on the main stem (TRIFL) was increased (Supplemental Table S2).

As indicated, flowering of amaranth was indeterminate and panicles (equivalent to pods for CROPGRO-Faba bean) appear before flowering. Therefore, a “false” anthesis date

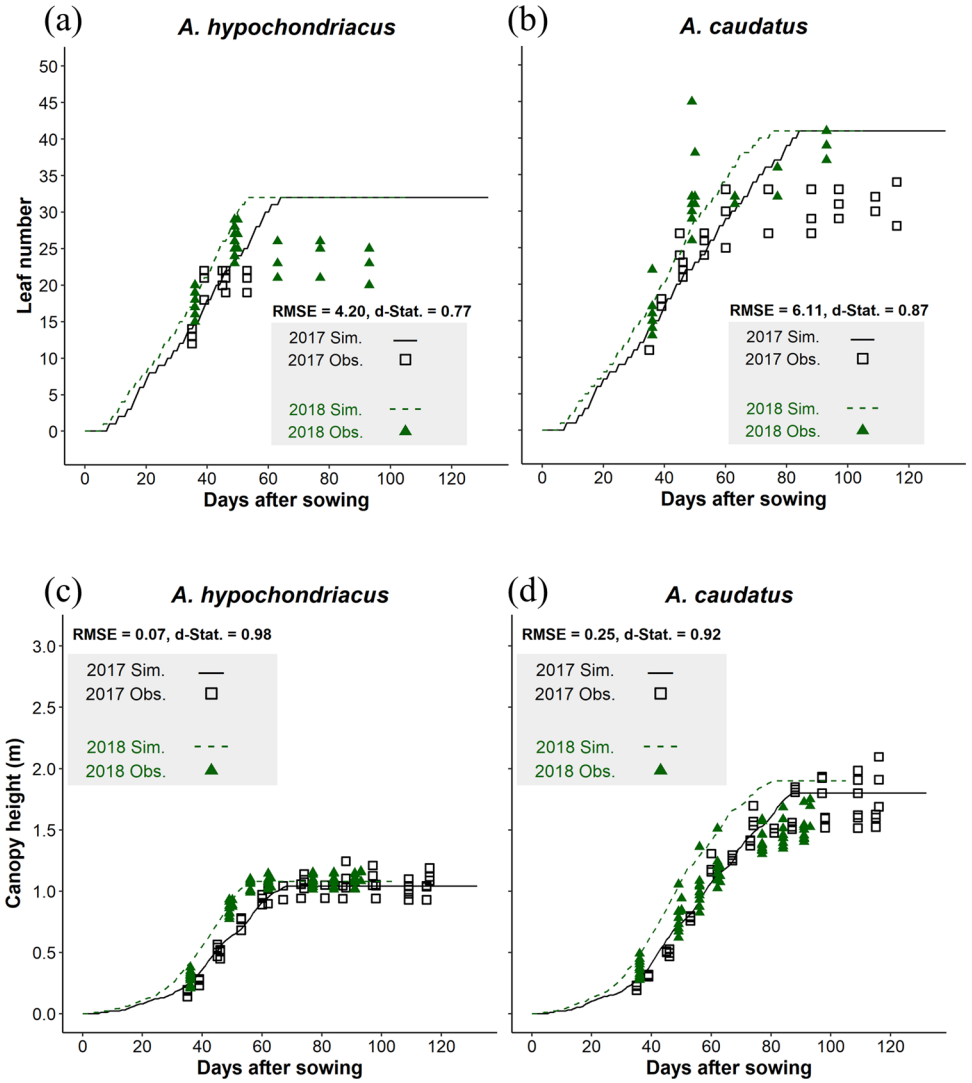

FIGURE 2 Simulated (Sim.) in comparison to observed (Obs.) values in 2017 and 2018 for (a, b) leaf number on the main stem and (c, d) canopy height for *Amaranthus hypochondriacus* L. Neuer Typ and *A. caudatus* L. K63. d-Stat., Willmott agreement index

was set so as to predict panicle occurrence and subsequently prediction of first seed. For NT the predicted and observed date of seed set in 2017 were 54 and 60 DAS and in 2018, 45 and 50 DAS, respectively. For K63, the predicted and observed date of seed set in 2017 were 58 and 60 DAS and in 2018, 49 and 62 DAS, respectively. Although these *Amaranthus* spp. cultivars especially NT have been bred and adapted for cultivation in central Europe, the substantial indeterminate growth made it impossible to set a date for physiological and harvest maturity because shedding of mature seeds occurred parallel to seed development.

Figure 2 shows simulated canopy height over time. The RMSE of canopy height for NT and K63 were 0.07 and 0.25 m and the d-Stat. were 0.98 and 0.92, respectively. The lower RMSE and the higher d-Stat. for the simulated and observed canopy height for NT than for K63 could be explained by the greater homogeneity observed for NT plant height in comparison to K63. For instance, by the end of the growing season in both years 2017 (117 DAS) and 2018 (102 DAS), the mean and standard deviation of plant height for NT were 104 and 13 cm, whereas for K63 they were 154 and 30 cm, respectively.

3.2.2 | Specific leaf area and leaf area index

Figure 3 shows SLA. In 2017, the mean SLA (n = 27) for NT ranged from 196 to 227 $cm^2\ g^{-1}$ and for K63 it ranged from 194 to 215 $cm^2\ g^{-1}$. The SLA range for NT based on our field experiments was higher than the range 144–177 $cm^2\ g^{-1}$, which has been reported for NT in a previous study (Gimplinger & Kaul, 2009). Nevertheless, due to high heterogeneity, the RMSE of SLA were 31.4 $cm^2\ g^{-1}$ and 29.6 $cm^2\ g^{-1}$ and the d-Stat. were 0.39 and 0.20 for NT and

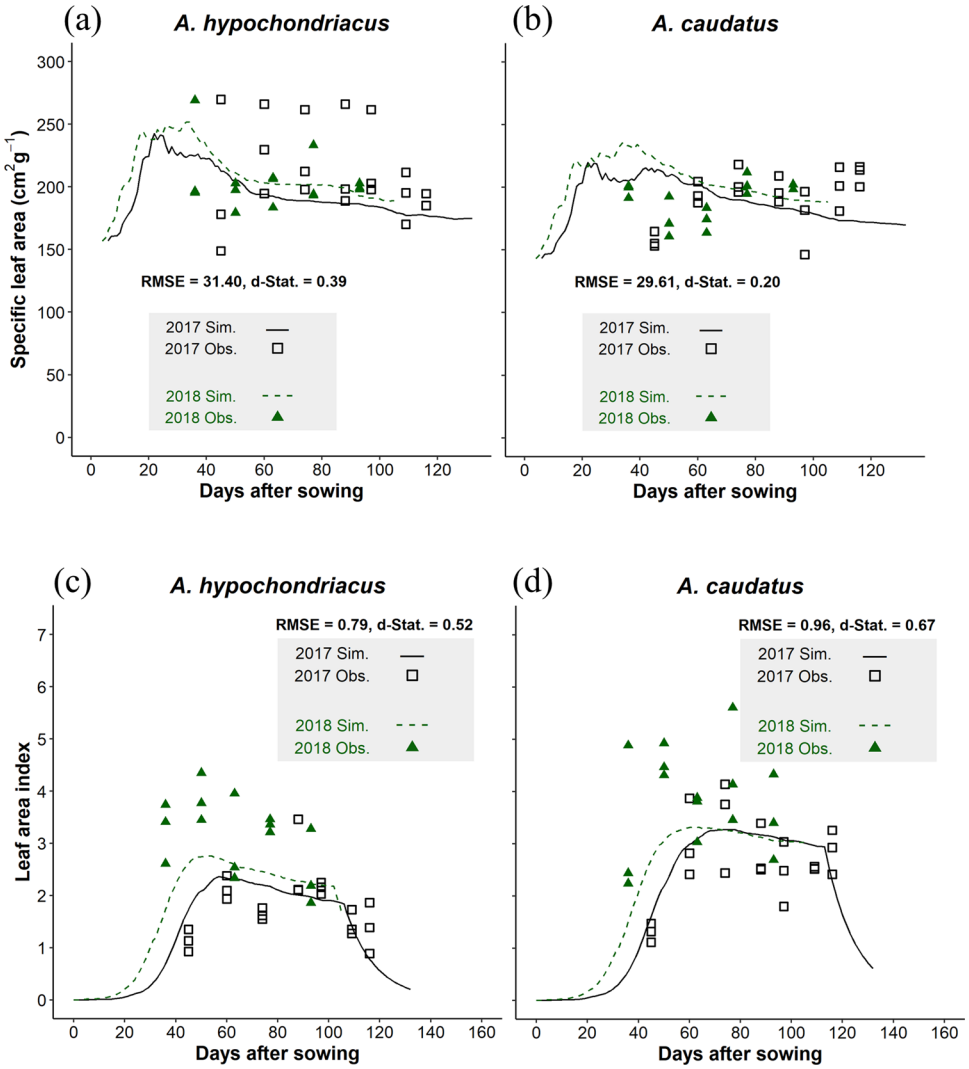

FIGURE 3 Simulated (Sim.) in comparison to observed (Obs.) values in 2017 and 2018 for (a, b) specific leaf area and (c, d) leaf area index for *Amaranthus hypochondriacus* L. Neuer Typ and *A. caudatus* L. K63. d-Stat., Willmott agreement index

K63, respectively (Figure 3a and 3b). A distinction was made between the amaranth varieties by setting the SLA under standard growth conditions (SLAVR) in the .CUL file for NT that had larger leaves to 230 cm^2 g^{-1} and for K63 to 210 cm^2 g^{-1}.

To adequately predict LAI, correct simulations for SLA and leaf biomass are required. Therefore, the vegetative partitioning parameters XLEAF, YLEAF, and YSTEM in the .SPE file were modified to allocate a lower fraction of dry matter to the leaves and stem from V15 to V45 onwards and more to the root (Supplemental Table S2). The RMSE of LAI for NT and K63 were 0.79 and 0.96 and the d-Stat. were 0.52 and 0.67, respectively (Figure 3c,d). Nevertheless, the RMSE of 0.79 for NT was much lower than the value RMSE of 1.16, which was reported for NT averaged across 2 yr after the calibration of the crop growth model LINTUL (Gimplinger & Kaul, 2009). The high RMSE and the low d-Stat. may be explained by the high heterogeneity in the observations among plants within the same cultivar. Incomplete domestication or weak domestication syndrome has been well reported as the main reason for phenotypic heterogeneity and intraspecific polymorphism in *Amaranthus* spp. (Stetter, 2016; Stetter et al., 2017).

3.2.3 | Biomass partitioning to leaf, stem, and panicle

Simulated leaf and stem weights are shown in Figure 4. The two seasons were quite different, with observed LAI, leaf, and stem mass being much higher in 2018 than in 2017. The RMSE of leaf weight for NT and K63 were 401 and 566 kg ha^{-1} and the d-Stat. were 0.60 and 0.65, respectively (Figure 4a,b). The RMSE of stem weight for NT and K63 were 1,092 and 1,658 kg ha^{-1} and the d-Stat. were 0.69 and 0.87, respectively (Figure 4c,d). Like for SLA and LAI, there was high variability in the leaf and stem weight within each of the *Amaranthus* spp. cultivars.

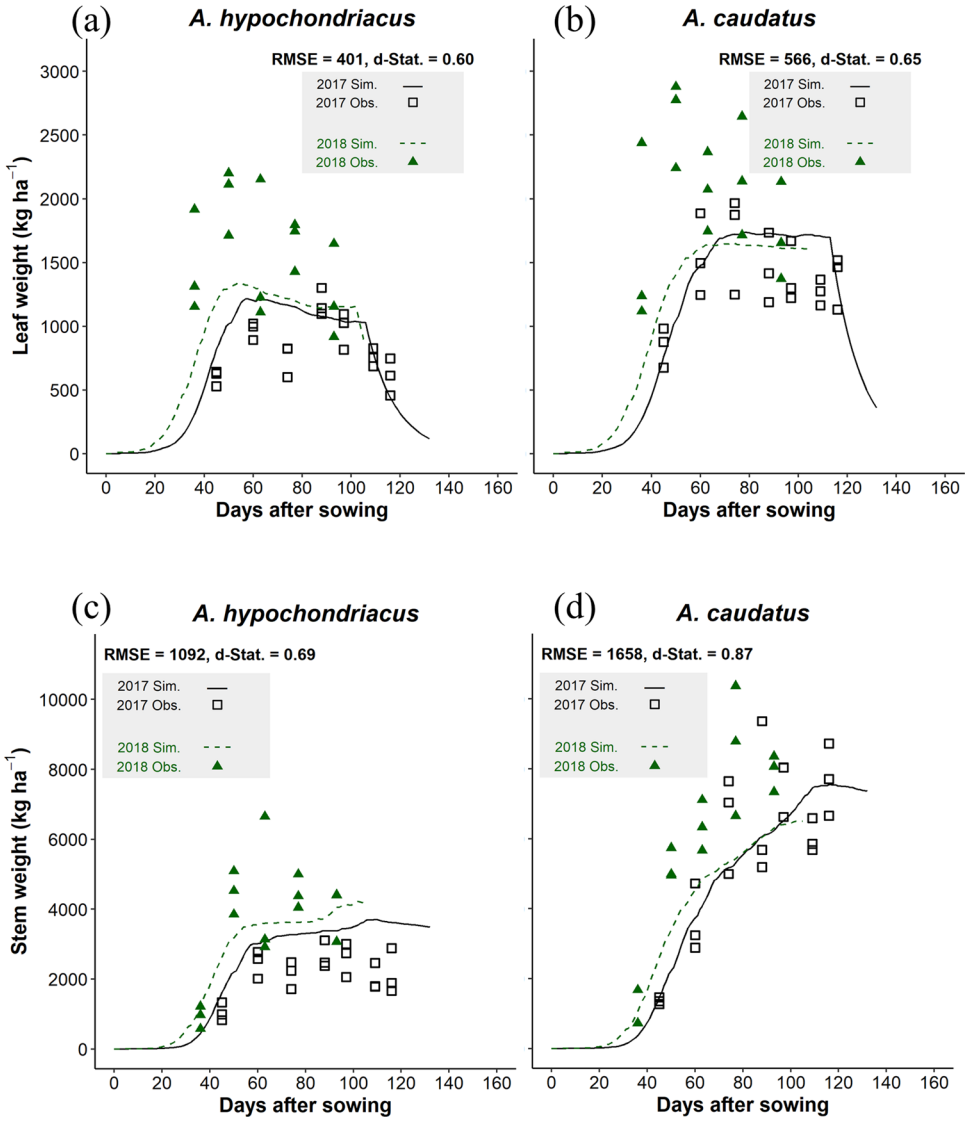

FIGURE 4 Simulated (Sim.) in comparison to observed (Obs.) values in 2017 and 2018 for (a, b) leaf and (c, d) stem weight for *Amaranthus hypochondriacus* L. Neuer Typ and *A. caudatus* L. K63. d-Stat., Willmott agreement index

The RMSE of panicle weight for NT and K63 were 2,034 and 1,153 kg ha^{-1}and the d-Stat. were 0.92 and 0.94, respectively (Figure 5a,b). For grain weight, the RMSE were 2,021 and 1,355 kg ha^{-1} and the d-Stat. were 0.21 and 0.46 for NT and K63, respectively (Figure 5c,d). In comparison a lower RMSE of 850 kg ha^{-1} (average of 2 yr of 112 and 57.9 g m^{-2}) for grain weight in NT was reported by (Gimplinger & Kaul, 2009) reported. As part of the calibration, we noticed that the T_{base} and $T_{opt}1$ of the quadratic functions driving the effect of temperature on pod (panicle) addition and seed growth had to be increased from the default values for faba bean (Table 4). This is also consistent with *Amaranthus* being a more warm-season species than faba bean.

As shown in Figure 5, the final harvest grain weight is less than the values measured at previous sampling dates due to substantial seed shattering especially for NT. There is a known problem of seed shattering in *Amaranthus* spp. (Gimplinger et al., 2008) that was also observed in our field trials in both years, so the calibration of seed weight could not be further optimized. However, if an earlier destructive sampling date had been chosen as the final harvest date, the RMSE for grain weight would also be reduced. Based on this finding, it may be recommended to harvest the grain up to 20 d earlier. Nevertheless, it is important to note that a high moisture content in stems and leaves at an earlier harvest date may severely reduce the effectiveness of threshing by a combine harvester.

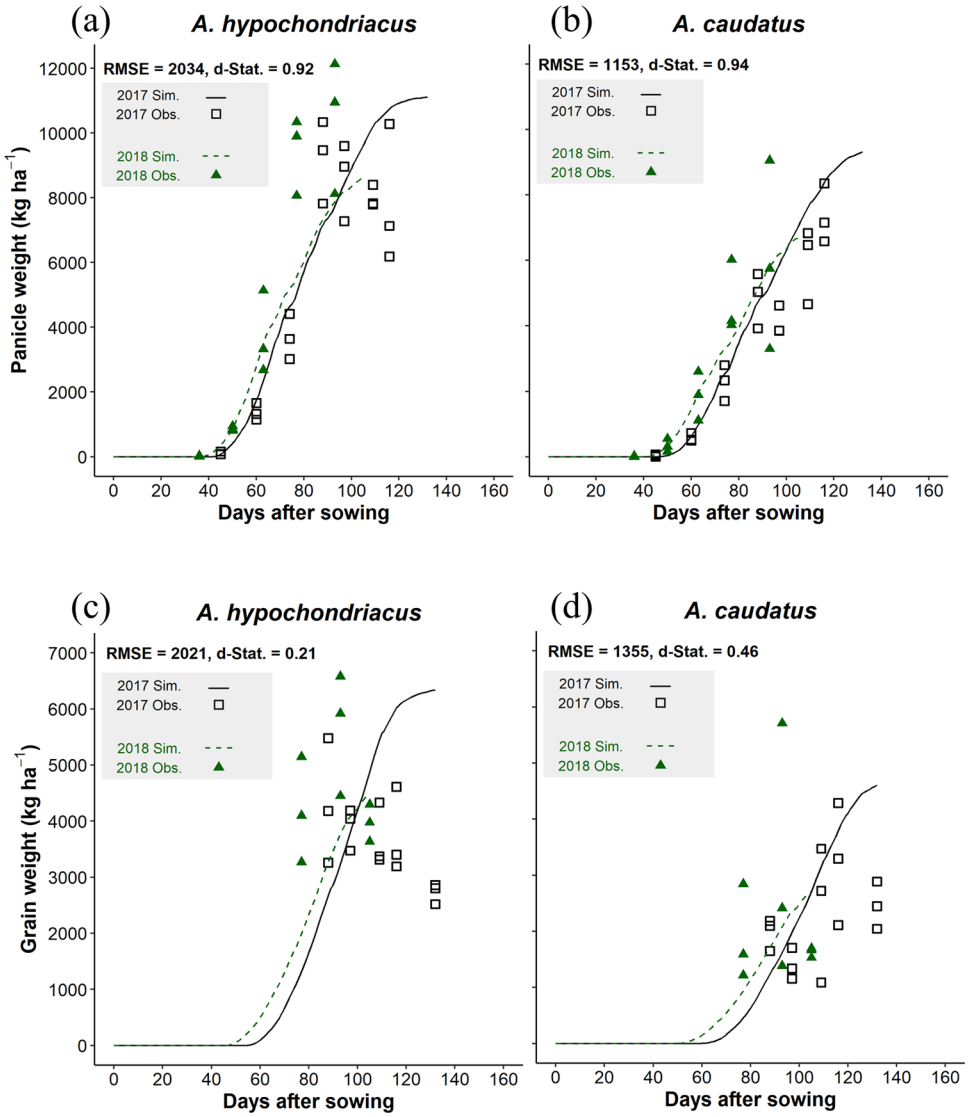

FIGURE 5 Simulated (Sim.) in comparison to observed (Obs.) values in 2017 and 2018 for (a, b) panicle and (c, d) grain weight for *Amaranthus hypochondriacus* L. Neuer Typ and *A. caudatus* L. K63. d-Stat., Willmott agreement index

3.2.4 | Panicle harvest index, grain harvest index, and grain/panicle ratio

Panicle (Panicle HI) and grain (HI) harvest indices and grain/panicle ratio, because they are plant-internal ratios, are not biased by sample size, which can be large or small randomly (Boote et al., 2002). Therefore, these variables illustrated in Figure 6 represent valuable variables for model calibration. As expected, in comparison to the individual organ weights, the RMSE for these ratios were low and the d-Stat. were high. The RMSE of panicle HI for NT and K63 were 0.05 and 0.06 and the d-Stat. were 0.99 and 0.96, respectively (Figure 6a,b). For HI, the RMSE were 0.065 and 0.060 and the d-Stat. were 0.59 and 0.56 for NT and K63, respectively (Figure 6c,d). The lower *d*-Stat for HI was influenced by differential shattering over time.

The RMSE of the percentage grain/panicle ratio (%) for NT and K63 were 7.88 and 10.12%, respectively, and the d-Stat. were 0.53 and 0.61, respectively (Supplemental Figure S1).

3.2.5 | Nitrogen mobilization and N concentration in plant organs

The parameters that drive the processes related to leaf senescence, C and N remobilization (SENRTE, SENPOR, CMOBMX, NVSMOB, and NMOBMX) were calibrated to optimize the simulated N concentrations in leaf, stem, and shell (panicle minus grain) and grain. As shown in Figure 7, the N concentration of leaf and stem decline over time and the model is capable to mimic that decline driven by N mobilization from vegetative to reproductive organs. The RMSE

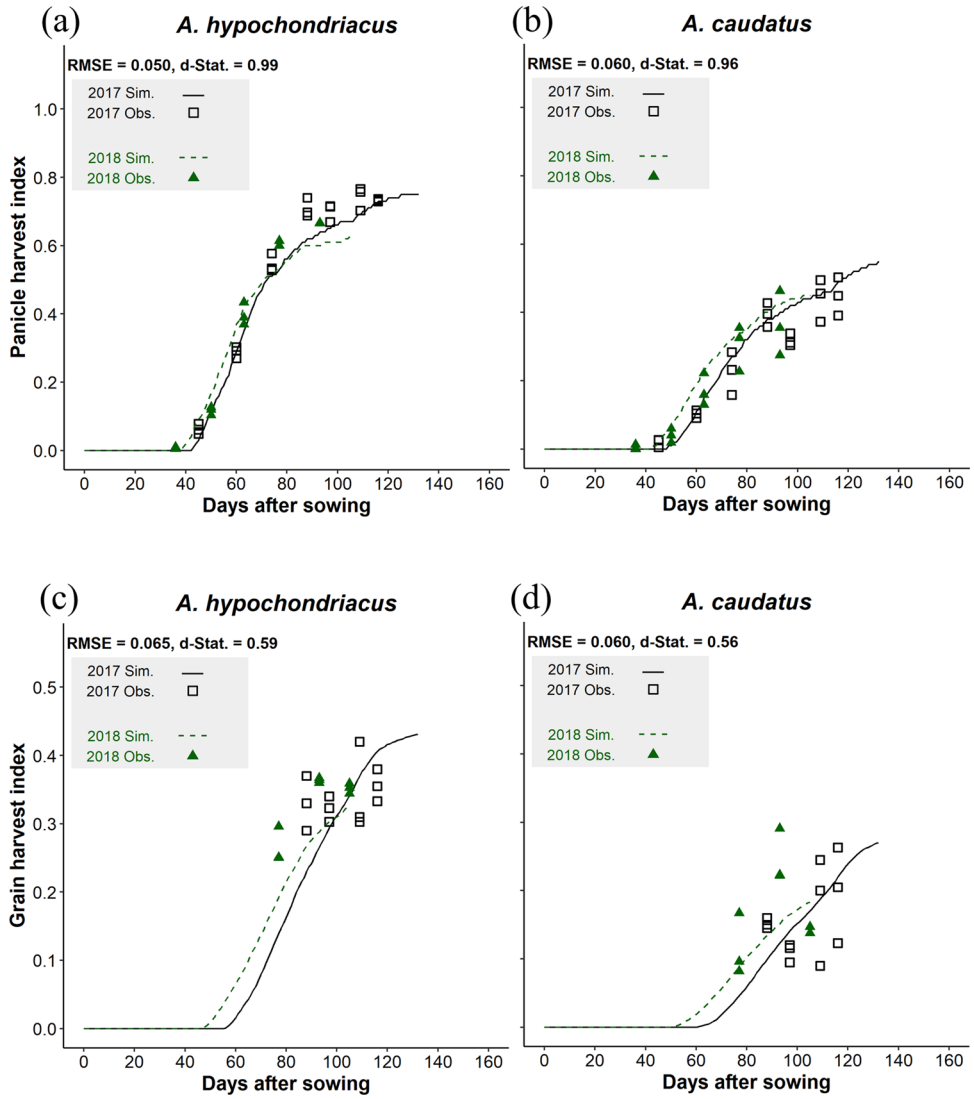

FIGURE 6 Simulated (Sim.) in comparison to observed (Obs.) values in 2017 and 2018 for (a, b) panicle harvest index (a, b) and (c, d) grain harvest index for *Amaranthus hypochondriacus* L. Neuer Typ and *A. caudatus* L. K63. d-Stat., Willmott agreement index

of leaf N concentration for NT and K63 were 0.38 and 0.40 and the d-Stat. were 0.94 and 0.92, respectively. For stem N concentration, the RMSE for NT and K63 were 0.88 and 0.82 and the d-Stat. were 0.69 and 0.65, respectively. Supplemental Figure S2 shows that the RMSE of shell N concentration for NT and K63 were 0.67 and 0.64 and the d-Stat. were 0.84 and 0.81, respectively. For grain N concentration, the RMSE for NT and K63 were 0.20 and 0.43 and the d-Stat. were 0.30 and 0.45, respectively.

3.2.6 | Aboveground biomass and N content

Finally, as shown in in Figure 8, the model successfully predicted biomass increase over time, with RMSE for NT and K63 of 2,948 and 2,572 kg ha^{-1} and the d-Stat. of 0.88 and 0.91, respectively (Figure 8a,b). For NT, a total biomass RMSE of 1,138 (average of 2 yr 135.7 and 91.8 g m^{-2}) has been reported (Gimplinger & Kaul, 2009), which is less than observed in this study. The RMSE of total aboveground biomass N for NT and K63 were 85.2 and 87.8 kg N ha^{-1} and the d-Stat. were 0.63 and 0.55, respectively (Figure 8c,d). For aboveground biomass and N content, the high RMSE and the low d-Stat. may be explained by the large variability in field observations, which can be, generally speaking, reduced by improved domestication of *Amaranthus* ssp. for more homogeneity.

As indicated previously, model adaptations were performed to simulate the growth of *Amaranthus* spp. using LINTUL 1 (Gimplinger & Kaul, 2009) and AquaCrop (Bello & Walker, 2017; Nyathi et al., 2018). LINTUL is a very simple crop model that relies on intercepted solar radiation and light use efficiency to describe growth and harvest index to partition dry matter (Spitters, 1990). In comparison to the CROPGRO model, which seems initially complex and requires adjustments to several parameters that drive crop growth at process

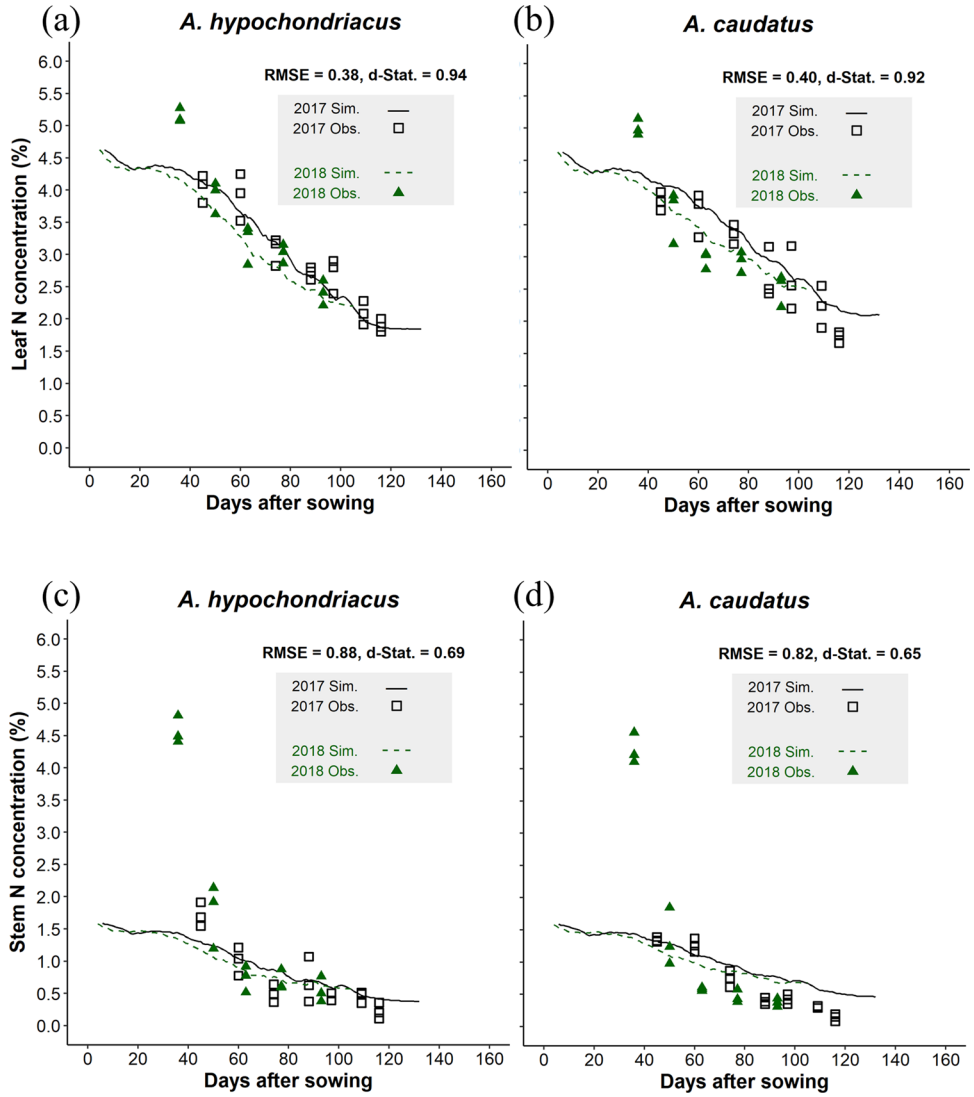

FIGURE 7 Simulated (Sim.) in comparison to observed (Obs.) values in 2017 and 2018 for (a, b) leaf and (c, d) stem N concentration for *Amaranthus hypochondriacus* L. Neuer Typ and *A. caudatus* L. K63. RMSE, root mean square error; d-Stat., Willmott agreement index

level and has greater complexity (e.g., leaf level photosynthesis) and temporal resolution (hourly and daily scales for different processes), the AquaCrop model is simple, founded on physically variables, requires fewer inputs and it uses mainly daily crop transpiration to drive biomass gain and, like for LINTUL, it also uses harvest index to determined reproductive yield (Steduto et al., 2009). Nevertheless, adaptation of CROPGRO for *Amaranthus* spp. offers a better understanding and integration of physiological processes than allowed by those two models.

4 | CONCLUSION

This study describes the first successful adaptation of a crop growth model for *Amaranthus* ssp. that is based on physiological processes that drive crop growth and development at a high spatio-temporal resolution. This was achieved by adapting the CROPGRO model by modifying the parameters that drive different physiological processes based on experimental observations in two contrasting years, published literature data or assumed values to achieve the best prediction of experimental data. Many parameters for plant physiological processes described by the default faba bean template of the CROPGRO-Faba bean model were retained regardless of the apparent complexity of the model adaptation process. Nevertheless, important aspects of the model adaptation included: changing the cardinal temperatures from a relatively cool-season faba bean crop to a warm-season amaranth crop the T_{base} and $T_{opt}1$ for vegetative, early, and late reproductive development were about 8 ˚C higher for amaranth than for faba bean. In that sense, the amaranth parameters are closer to that of soybean a warm-season crop. Photoperiod sensitivity was turned "off" and crop and

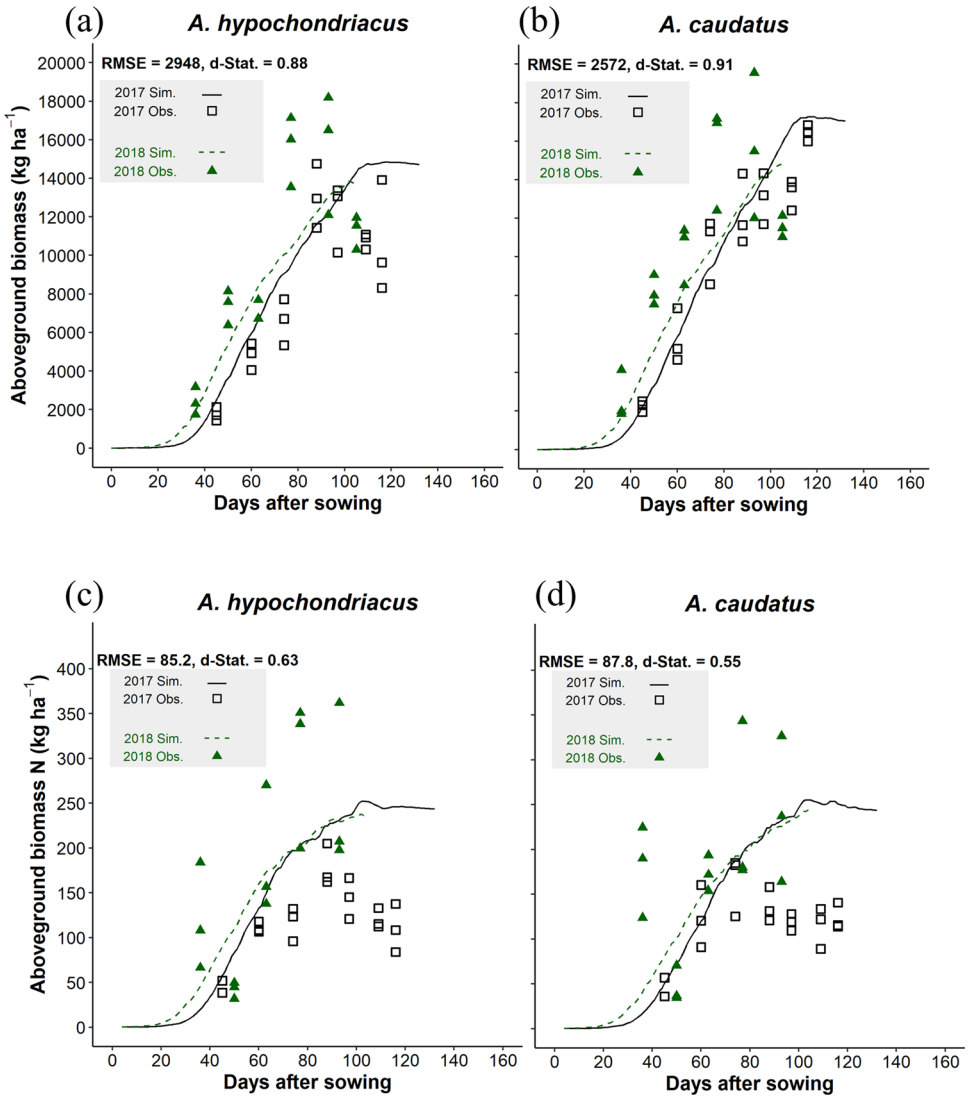

FIGURE 8 Simulated (Sim.) in comparison to observed (Obs.) values in 2017 and 2018 for (a, b) aboveground biomass and (c, d) aboveground biomass N content for *Amaranthus hypochondriacus* L. Neuer Typ and *A. caudatus* L. K63. RMSE, root mean square error; d-Stat., Willmott agreement index

cultivar parameters in the species (.SPE), cultivar (.CUL), and ecotype (.ECO) files were modified to successfully simulate the duration of phenological phases, vegetative and reproductive partitioning, C and N mobilization, and maturity. In doing so, the standard FORTRAN code of the CROPGRO model remained unchanged. Across both *Amaranthus* spp., the model adaptation led to very good predictions (d-Stat. ≥ 0.9) of canopy height, panicle weight, panicle harvest index, leaf N concentration, and aboveground biomass. Despite substantial intraspecific polymorphism (plant to plant variability) in *Amaranthus* spp. due to incomplete domestication, which could be confirmed by the high heterogeneity observed in plant traits in the field trials, the predictions of leaf number, LAI, leaf and stem weight, stem and shell N concentration, and aboveground biomass N content were good to moderate (d-Stat. ≥ 0.6 – 0.9). A strength of this model adaptation is that it is based on two phenological different amaranth varieties that were grown in two contrasting cropping years (different average temperatures and cumulative precipitation). Like for quinoa (Präger et al., 2019), a modification of the model code may be required to simulate tiny seeds and improve partitioning in the reproductive phase. Additionally, evaluation of the model with new data from different locations with contrasting weather conditions and under different management practices (sowing date, plant density, row distance, N fertilization) would contribute to test its robustness. Therefore, it is recommended to make this model available for testing and improvement in the next DSSAT package release. The availability of "CROPGRO-Amaranth" in DSSAT will further support research in breeding and crop management to improve the establishment of grain *Amaranthus* as a "superfood" crop with a low to moderate N requirement and

substantial tolerance to drought in cropping systems in central Europe and around the world.

ACKNOWLEDGMENTS

The authors are grateful for the support provided by the staff of Ihinger Hof (an experimental station of the University of Hohenheim) in the management of the field experiments and to student assistance for their help in the field. Thanks go particularly to Aline Breuninger, Martin Zahner, Sebastian Bökle, Samuel Ateba and Abdullah Al. Mamun. This research was funded by the German Federal Ministry for Economic Affairs and Energy within the Central Innovation Program for SMEs, grant no. 16KN050528.

AUTHOR CONTRIBUTIONS

Peteh Mehdi Nkebiwe: Conceptualization; Data curation; Formal analysis; Investigation; Methodology; Resources; Software; Validation; Visualization; Writing-original draft; Writing-review & editing. Ken Boote: Conceptualization; Methodology; Resources; Software; Supervision; Validation; Writing – review & editing. Annegret Pflugfelder: Conceptualization; Investigation; Methodology; Writing – review & editing. Sebastian Munz: Conceptualization; Methodology; Software; Supervision; Writing – review & editing. Simone Graeff-Hönninger: Conceptualization; Funding acquisition; Methodology; Project administration; Resources; Supervision; Writing – review & editing.

CONFLICT OF INTEREST

The authors declare no conflict of interest. The funders had no role in the design of the study; in the collection, analyses, or interpretation of data; in the writing of the manuscript, or in the decision to publish the results.

ORCID

Peteh Mehdi Nkebiwe https://orcid.org/0000-0002-0344-0509
Ken Boote https://orcid.org/0000-0002-1358-5496
Sebastian Munz https://orcid.org/0000-0001-6713-1863
Simone Graeff-Hönninger https://orcid.org/0000-0001-9996-961X

REFERENCES

Alemayehu, F. R., Bendevis, M. A., & Jacobsen, S.-E. (2015). The potential for utilizing the seed crop amaranth (*Amaranthus* spp.) in East Africa as an alternative crop to support food security and climate change Mitigation. *Journal of Agronomy and Crop Science*, *201*(5), 321–329. https://doi.org/10.1111/jac.12108

Alvarez-Jubete, L., Arendt, E. K., & Gallagher, E. (2009). Nutritive value and chemical composition of pseudocereals as gluten-free ingredients. *International Journal of Food Sciences and Nutrition*, *60*(sup4), 240–257. https://doi.org/10.1080/09637480902950597

Alvarez-Jubete, L., Arendt, E. K., & Gallagher, E. (2010). Nutritive value of pseudocereals and their increasing use as functional gluten-free ingredients. *Trends in Food Science & Technology*, *21*(2), 106–113. https://doi.org/10.1016/j.tifs.2009.10.014

Association of Official Analytical Chemists (AOAC). (1990). *Official methods of analysis* (15th ed.). Association of Official Analytical Chemists.

Assad, R., Reshi, Z. A., Jan, S., & Rashid, I. (2017). Biology of amaranths. *The Botanical Review*, *83*(4), 382–436. https://doi.org/10.1007/s12229-017-9194-1

Bello, Z. A., & Walker, S. (2017). Evaluating AquaCrop model for simulating production of amaranthus (*Amaranthus cruentus*) a leafy vegetable, under irrigation and rainfed conditions. *Agricultural and Forest Meteorology*, *247*, 300–310. https://doi.org/10.1016/j.agrformet.2017.08.003

Boote, K. J. (1999). Concepts for calibrating crop growth models. In G. Hoogenboom, P. W. Wilkens, & G. Y. Tsuji (Eds.), *DSSAT v3* (Volume 4, pp. 179–199). University of Hawaii.

Boote, K. J., Jones, J. W., & Hoogenboom, G. (1998). Simulation of crop growth: CROPGRO model. In R. Peart & R. Curry (Eds.), *Agricultural systems modeling and simulation* (pp. 651–692). Marcel Dekker.

Boote, K. J., Jones, J. W., Hoogenboom, G., & Pickering, N. B. (1998). The CROPGRO model for grain legumes. In G. Tsuji & et al. (Eds.), *Understanding options for agricultural production* (pp. 99–128). Kluwer Academic Publishing.

Boote, K. J., Mínguez, M. I., & Sau, F. (2002). Adapting the CROPGRO legume model to simulate growth of faba bean. *Agronomy Journal*, *94*(4), 743–756. https://doi.org/10.2134/agronj2002.7430

Bora, G. C. (2018). Amaranthus (Pigweed). In Md. Hedayetullah & P. Zaman (Eds.), *Forage crops of the world, Volume II: Minor forage crops* (pp. 253–266). Apple Academic Press.

Caselato-Sousa, V. M., & Amaya-Farfán, J. (2012). State of knowledge on amaranth grain: A comprehensive review. *Journal of Food Science*, *77*(4), 93–104. https://doi.org/10.1111/j.1750-3841.2012.02645.x

Confederation of British Industry (CBI). (2021). *What is the demand for grains, pulses and oilseeds on the European market?* Confederation of British Industry (CBI). https://www.cbi.eu/market-information/grains-pulses-oilseeds/trade-statistics

Chang, Y.-C., Chiu, Y.-C., Tsao, N.-W., Chou, Y.-L., Tan, C.-M., Chiang, Y.-H., Liao, P.-C., Lee, Y.-C., Hsieh, L.-C., Wang, S.-Y., & Yang, J.-Y. (2021). Elucidation of the core betalain biosynthesis pathway in *Amaranthus tricolor*. *Scientific Reports*, *11*(1), 6086. https://doi.org/10.1038/s41598-021-85486-x

Di Paola, A., Valentini, R., & Santini, M. (2016). An overview of available crop growth and yield models for studies and assessments in agriculture. *Journal of the Science of Food and Agriculture*, *96*(3), 709–714. https://doi.org/10.1002/jsfa.7359

El-Sharkawy, M. A., Loomis, R. S., & Williams, W. A. (1968). Photosynthetic and respiratory exchanges of carbon dioxide by leaves of the grain amaranth. *Journal of Applied Ecology*, 243–251. https://doi.org/10.2307/2401288

Fuller, H. J. (1949). Photoperiodic responses of *Chenopodium quinoa* Willd. and *Amaranthus caudatus* L. *American Journal of Botany*, *36*(2), 175–180. https://doi.org/10.2307/2437786

Gimplinger, D. M., Dobos, G., Schonlechner, R., & Kaul, H. (2007). Yield and quality of grain amaranth (*Amaranthus* sp.) in eastern

Austria. *Plant Soil and Environment*, *53*(3), 105. https://doi.org/10.17221/2224-PSE

Gimplinger, D. M., & Kaul, H. P. (2009). Calibration and validation of the crop growth model LINTUL for grain amaranth (*Amaranthus* sp.). *Journal of Applied Botany and Food Quality*, *82*(2), 183–192.

Gimplinger, D. M., Schulte auf'm Erley, G., Dobos, G., & Kaul, H.-P. (2008). Optimum crop densities for potential yield and harvestable yield of grain amaranth are conflicting. *European Journal of Agronomy*, *28*(2), 119–125. https://doi.org/10.1016/j.eja.2007.05.007

He, D., Wang, E., Wang, J., & Robertson, M. J. J. (2017). Data requirement for effective calibration of process-based crop models. *Agricultural and Forest Meteorology*, *234-235*, 136–148. https://doi.org/10.1016/j.agrformet.2016.12.015

Hoogenboom, G., Justes, E., Pradal, C., Launay, M., Asseng, S., Ewert, F., & Martre, P. (2021). iCROPM 2020: Crop modeling for the future. *Journal of Agricultural Science*, *158*(10), 791–793. https://doi.org/10.1017/S0021859621000538

Hoogenboom, G., Porter, C. H., Shelia, V., Boote, K. J., Singh, U., White, J., Hunt, L. L. A., Ogoshi, R., Lizaso, J., Koo, J., Asseng, S., Singels, A., Moreno, L., & Jones, J. W. (2019). *Decision support system for agrotechnology transfer (DSSAT)* (Version 4.7.5). https://DSSAT.net

IUSS Working Group WRB. (2007). *World Reference Base for Soil Resources 2006, first update 2007* (World Soil Resources Reports 103). FAO.

Jacobsen, S. E., Mujica, A., & Ortiz, R. (2003). The global potential for quinoa and other Andean crops. *Food Reviews International*, *19*(1-2), 139–148. https://doi.org/10.1081/FRI-120018880

Johnson, B. L., & Henderson, T. L. (2002). Water use patterns of grain amaranth in the northern Great Plains. *Agronomy Journal*, *94*(6), 1437–1443. https://doi.org/10.2134/agronj2002.1437

Jones, J. W., Antle, J. M., Basso, B., Boote, K. J., Conant, R. T., Foster, I., Godfray, H. C. J., Herrero, M., Howitt, R. E., Janssen, S., Keating, B. A., Munoz-Carpena, R., Porter, C. H., Rosenzweig, C., & Wheeler, T. R. (2017). Brief history of agricultural systems modeling. *Agricultural Systems*, *155*, 240–254. https://doi.org/10.1016/j.agsy.2016.05.014

Jones, J. W., Hoogenboom, G., Porter, C. H., Boote, K. J., Batchelor, W., Hunt, L. L. A., Wilkens, P., Singh, U., Gijsman, A., & Ritchie, J. (2003). The DSSAT cropping system model. *European Journal of Agronomy*, *18*(3), 235–265. https://doi.org/10.1016/S1161-0301(02)00107-7

Krähmer, H. (2016). Can we associate weeds with specific environmental conditions? In H. Krähmer (Ed.), *Atlas of weed mapping* (pp. 139–160). Wiley Blackwell.

Mack, L., Boote, K. J., Munz, S., Phillips, T. D., & Graeff-Hönninger, S. (2020). Adapting the CROPGRO model to simulate chia growth and yield. *Agronomy*, *112*(5), 3859–3877. https://doi.org/10.1002/agj2.20305

Martínez-Núñez, M., Ruiz-Rivas, M., Vera-Hernández, P. F., Bernal-Muñoz, R., Luna-Suárez, S., & Rosas-Cárdenas, F. F. (2019). The phenological growth stages of different amaranth species grown in restricted spaces based in BBCH code. *South African Journal of Botany*, *124*, 436–443. https://doi.org/10.1016/j.sajb.2019.05.035

Meier, U., Bleiholder, H., Buhr, L., Feller, C., Hack, H., Heß, M., Lancashire, P. D., Schnock, U., Stauß, R., & van den Boom, T. (2009). The BBCH system to coding the phenological growth stages of plants–History and publications. *Journal Für Kulturpflanzen*, *61*(2), 41–52. https://doi.org/10.5073/JfK.2009.02.01

Mlosch, L. (2015). *Einfluss von Inhaltsstoffen und Kornparametern verschiedener Amarantsorten auf die Aufpoppfähigkeit im industriellen Maßstab* (In German) [Master's thesis, University of Hohenheim].

Myers, R. L. (1998). Nitrogen fertilizer effect on grain amaranth. *Agronomy Journal*, *90*(5), 597–602. https://doi.org/10.2134/agronj1998.00021962009000050005x

Nyathi, M. K., van Halsema, G. E., Annandale, J. G., & Struik, P. C. (2018). Calibration and validation of the AquaCrop model for repeatedly harvested leafy vegetables grown under different irrigation regimes. *Agricultural Water Management*, *208*, 107–119. https://doi.org/10.1016/j.agwat.2018.06.012

Pandey, R. M., & Singh, R. (2009). Genetic improvement of grain amaranths: A review. *Current Advances in Agricultural Sciences*, *1*(2), 61–64.

Präger, A., Boote, K. J., Munz, S., & Graeff-Hönninger, S. (2019). Simulating growth and development processes of quinoa (*Chenopodium quinoa* Willd.): Adaptation and evaluation of the CSM-CROPGRO model. *Agronomy*, *9*(12), 832. https://doi.org/10.3390/agronomy9120832

Sarker, U., Islam, M. T., Rabbani, M. G., & Oba, S. (2018). Variability in total antioxidant capacity, antioxidant leaf pigments and foliage yield of vegetable amaranth. *Journal of Integrative Agriculture*, *17*(5), 1145–1153. https://doi.org/10.1016/S2095-3119(17)61778-7

Scholberg, J., Boote, K. J., Jones, J. W., & McNeal, B. (1997). Adaptation of the CROPGRO model to simulate the growth of field-grown tomato. In M. Kropff, P. S. Teng, P. K. Aggarwal, J. Bouma, B. A. M. Bouman, J. W. Jones, & H. H. Laar (Eds.), *Applications of systems approaches at the field level. Systems approaches for sustainable agricultural development* (Vol. 6, pp. 135–151). Springer. https://doi.org/10.1007/978-94-017-0754-1_9

Singh, S., Boote, K. J., Angadi, S. V., Grover, K., Begna, S., & Auld, D. (2016). Adapting the CROPGRO Model to simulate growth and yield of spring safflower in semiarid conditions. *Agronomy Journal*, *108*(1), 64–72. https://doi.org/10.2134/agronj15.0272

Soriano-García, M., & Aguirre-Díaz, I. S. (2019). Nutritional functional value and therapeutic utilization of amaranth. In V. Y. Waisundara (Ed.), *Nutritional value of amaranth*. IntechOpen.

Spinoni, J., Vogt, J. V., Naumann, G., Barbosa, P., & Dosio, A. (2018). Will drought events become more frequent and severe in Europe? *International Journal of Climatology*, *38*(4), 1718–1736. https://doi.org/10.1002/joc.5291

Spitters, C. (1990). Crop growth models: Their usefulness and limitations. *Acta Horticulturae*, *267*, 349–368. https://doi.org/10.17660/ActaHortic.1990.267.42

Steberl, K., Boote, K. J., Munz, S., & Graeff-Hönninger, S. (2020). Modifying the CROPGRO Safflower model to simulate growth, seed and floret yield under field conditions in southwestern Germany. *Agronomy*, *10*(1), 11. https://doi.org/10.3390/agronomy10010011

Steduto, P., Raes, D., Hsiao, T. C., Fereres, E., Heng, L. K., Howell, T. A., Evett, S. R., Rojas-Lara, B. A., Farahani, H. J., & Izzi, G. (2009). Concepts and applications of AquaCrop: The FAO crop water productivity model. In W. Cao, J. White, & E. Wang (Eds.), *Crop modeling and decision support* (pp. 175–191). Springer. https://doi.org/10.1007/978-3-642-01132-0_19

Stetter, M. G. (2016). *Speciation and domestication genomics of Amaranthus spp* [Doctoral dissertation, University of Hohenheim]. http://opus.uni-hohenheim.de/volltexte/2017/1312/

Stetter, M. G., Müller, T., & Schmid, K. J. (2017). Genomic and phenotypic evidence for an incomplete domestication of South American

grain amaranth (*Amaranthus caudatus*). *Molecular Ecology*, *26*(3), 871–886. https://doi.org/10.1111/mec.13974

Stetter, M. G., Vidal-Villarejo, M., & Schmid, K. J. (2019). Parallel seed color adaptation during multiple domestication attempts of an ancient new world grain. *Molecular Biology and Evolution*, *37*(5), 1407–1419. https://doi.org/10.1093/molbev/msz304

Übelhör, A., Munz, S., Graeff-Hönninger, S., & Claupein, W. (2015). Evaluation of the CROPGRO model for white cabbage production under temperate European climate conditions. *Scientia Horticulturae*, *182*, 110–118. https://doi.org/10.1016/j.scienta.2014.11.019

Venskutonis, P. R., & Kraujalis, P. (2013). Nutritional components of amaranth seeds and vegetables: A review on composition, properties, and uses. *Comprehensive Reviews in Food Science and Food Safety*, *12*(4), 381–412. https://doi.org/10.1111/1541-4337.12021

Willmott, C. J. (1982). Some comments on the evaluation of model performance. *Bulletin of the American Meteorological Society*, *63*(11), 1309–1313. https://doi.org/10.1175/1520-0477

Wu, H., Sun, M., Yue, S., Sun, H., Cai, Y., Huang, R., Brenner, D., & Corke, H. (2000). Field evaluation of an *Amaranthus* genetic resource collection in China. *Genetic Resources and Crop Evolution*, *47*(1), 43–53. https://doi.org/10.1023/A:1008771103826

Zabka, G. G. (1961). Photoperiodism in *Amaranthus caudatus*. I. A Re-Examination of the photoperiodic response. *American Journal of Botany*, *48*(1), 21–28. https://doi.org/10.1002/j.1537-2197.1961.tb11599.x

SUPPORTING INFORMATION

Additional supporting information can be found online in the Supporting Information section at the end of this article.

How to cite this article: Nkebiwe, P. M., Boote, K., Pflugfelder, A., Munz, S., & Graeff-Hönninger, S. (2022). Adapting the CROPGRO-faba bean model to simulate the growth and development of *Amaranthus* species. *Agronomy Journal*, 1–21. https://doi.org/10.1002/agj2.21090